NATIONAL ADVISORY COMMITTEE FOR AERONAUTICS

TECHNICAL MEMORANDUM

No. 1203

THE COMPRESSIBLE FLOW PAST VARIOUS PLANE PROFILES NEAR SONIC VELOCITY

By B. Göthert and K. H. Kawalki

Translation of Untersuchungen und Mitteilungen Nr. 1471, 1945

NACA

Washington

March 1949

NATIONAL ADVISORY COMMITTEE FOR AERONAUTICS

TECHNICAL MEMORANDUM NO. 1203

THE COMPRESSIBLE FLOW PAST VARIOUS PLANE PROFILES NEAR SONIC VELOCITY*

By B. Göthert and K. H. Kawalki

SUMMARY

In an earlier report UM No. 1117 by Göthert, entitled "Berechnung kompressibler ebener Strömungen bei hohen Unterschall-Anblasegeschwindigkeiten" (Calculation of Compressible Plane Flows at High Subsonic Airspeeds), the single-source method was applied to the compressible flow around circles, ellipses, lunes and around an elongated body of revolution at different Mach numbers and the results compared as far as possible with the calculations by Lamla and Busemann. Essentially, it was found that with favorable source arrangement the single-source method is in good agreement with the calculations of the same degree of approximation by Lamla and Busemann. Near sonic velocity the number of steps must be increased considerably in order to sufficiently approximate the adiabatic curve. After exceeding a certain Mach number where local supersonic fields occur already, it was no longer possible, in spite of the substantially increased number of steps, to obtain a systematic solution because the calculation diverged. This result was interpreted to mean that above this point of divergence the symmetrical type of flow ceases to exist and changes into the unsymmetrical type characterized by compressibility shocks.

SURVEY OF THE APPROXIMATION METHOD USED

In report UM No. 1117, it is explained how by means of successive approximations the velocity field around plane profiles at high subsonic speeds can be computed. But instead of representing the solution in closed form as practiced in the conventional methods up to now, a numerical method was developed by which a large number of approximating steps can be computed, such that the labor for the individual step is not increased, with progressive degree of approximation. As a consequence, the restriction was removed of being able to compute, in general, only

---

*"Die kompressible Strömung um verschiedene ebene Profile in Nähe der Schallgeschwindigkeit." Zentrale für wissenschaftliches Berichtswesen der Luftfahrtforschung des Generalluftzeugmeisters (ZWB) Berlin-Adlershof, Untersuchungen und Mitteilungen Nr. 1471, January 6, 1945.

two individual approximations owing to the increasing amount of paper-work involved. On the other hand, however, it was taken into the bargain that even at increasing degree of approximation the "mesh width" of the numerical method is, in general, maintained, so that a small consistent residual error remains, but judged from the model problems worked out, this error remains, on the whole, far below the error introduced by an insufficient number of individual approximations.

The afore-mentioned report proceeds from the concept that the compressible flow can be regarded as a special incompressible flow, where the entire flow field outside of the profile in the stream is covered with elementary sources and sinks, the yield of which is dependent in a simple manner upon the magnitude of the local Mach number. Thus, if the velocity field around a profile were known, the elementary sources themselves would be known also. The departure of the compressible from the incompressible velocity distribution could then be explained simply by the fact that the additional velocities produced by the sum of the elementary sources are computed. By the method pursued in the subsequently described model problems, the elementary sources were determined first from the velocity field of the incompressible flow, that is, the velocity field of the Prandtl rule, and with this first approximation formula for the source intensities, the variations of the velocity field computed. With this improved velocity field, the source intensities are then computed again and from it the velocities until with progressive degree of approximation the additional velocities due to the sources tend toward a fixed value that represents the desired velocity in the respective point of the compressible-flow field.

As the calculation of the elementary sources for given velocity is comparatively simple, it is important that the velocity field, which is produced by the sources distributed two dimensionally over the entire flow field, be computed in the simplest possible manner. For this purpose, the incompressible comparative flow covered with sources is conformably transformed on the circular flow, where the individual elementary sources do not vary in yield. The two dimensionally distributed sources were combined into concentric rings or, for even rougher approximation, into single-point sources which were disposed in suitable manner at such points where the maximum yield of the sources is to be expected. Even this very rough method proved surprisingly satisfactory by suitably arranged single sources for defining the velocities in the proximity of maximum profile thickness as verified by a comparison with the known calculations of Lamla and Busemann with the substantially more accurate source ring method.

The present report deals with a number of model calculations for profile flows worked out by the single-source method. The number of single sources in each flow gradient was fixed at twelve, the choice

of arrangement being such that the single sources disposed along a stream filament are of equal yield as much as possible. The calculation was further simplified by postulating symmetrical flows. Unsymmetrical supersonic flows with compressibility shocks are thus ruled out beforehand.

One particular advantage of the single-source method consists in being able to see at once whether the chosen number of approximation steps already complies adequately with the continuity condition of the compressible flow or whether the method diverges and so indicates that, at the particular Mach number for the chosen profile, symmetrical flow free from compressibility shocks is no longer to be expected.

II. VELOCITY DISTRIBUTION ABOUT A LINE (CRESCENT) ($d/l = 0.10$)

1. Mach Numbers with Convergence of Computed Flows

The chosen single-source scheme (system I, appendix) for a crescent ($d/l = 0.10$) at $M_\infty = 0.77$ is represented in figure 1. The 12 single sources are arranged so as to lie particularly close together near the point of maximum profile thickness in order to be able to better account for the high yield of the sources expected here. But at greater distance from the profile, the sources are spaced farther apart because the total yield, owing to the already subsided increases of velocity and the reaction of these outer-lying sources to the velocities at the profile contour and on the areas of great source density, is substantially less. The additional velocities due to the single sources were computed in starting points disposed as much as possible at equal distance from the adjacent single sources in order to minimize the error due to the point concentration of the elementary sources. The represented source diagram varies with increasing Mach number so that the individual sources move farther outward into the flow. This outward travel of the sources, desirable from the physical standpoint, offers mathematically an alleviation or facility by reason of the fact that after application of the Prandtl rule, the source locations in the plane of flow, conformally transformed in a circle, are coincident for all Mach numbers so that the additional velocities induced by the sources in the plane of the circle can be computed with the aid of the same influence factor.

The result of the approximate calculation with the previously described system of sources and starting points at $M_\infty = 0.77$ is illustrated in figure 1; the stream density (ρv) is plotted against the Mach number for different groups of starting points; the correct value of the stream density striven for by the approximate calculation is given by the adiabatic curve which at sonic velocity $M^+ = 1$ has its maximum as sign for the greatest possible stream density. At point

$M^+ = M^+_\infty$, which corresponds to the state of the flow velocity, the adiabatic curve is tangent to the stream density curve of the Prandtl rule. On the Prandtl curve, all points of the approximate calculation by the Prandtl rule are located; they are identified in the diagram as 0^{th} approximation, such as the starting point 11 at the maximum velocity, etc., for example. The difference of the stream density in the particular approximation points relative to the accurate adiabatic curve indicates then the extent to which the stream density by Prandtl rule is still too great and to which the width of the stream filament passing through the respective starting point is still too small to fulfill the condition of continuity of the compressible flow. This difference represents, therefore, at the same time a measure for the additionally to be applied source yield, which is to force the particular stream filament apart to the correct width. On computing the additive velocities by the sources which are dimensional according to the velocity field of the Prandtl rule, (0^{th} approximation) the velocity field of the next higher is obtained or, in this case, of the first approximation. It is true that the points of the first approximation found this way lie already much closer to the adiabatic curve than to the Prandtl curve; but it is seen at once that the second degree of approximation, especially at the points of maximum velocities, is still not adequate to approximate the adiabatic curve closely enough. Since the still remaining difference relative to the adiabatic curve is immediately apparent from the diagram even for the points of the first approximation and the additive yield is thus known, the second approximation and also the higher approximations can be calculated at once. For the example in question, it is seen (fig. 1) that about five approximative steps are necessary to approximate the adiabatic curve accurately enough starting from Prandtl's curve.

The number of steps required is, of course, less at small Mach numbers of flow. Thus, figures 2 and 3 show, for example, that at $M_\infty = 0.75$ for the same profile only about three, and at $M_\infty = 0.70$ only about two steps are needed to attain the same degree of approximation as at $M_\infty = 0.77$ with five steps. On the other hand, the number of steps required at higher M increases enormously. From all these approximate calculations reproduced in figures 1 to 3, it is apparent that in the middle section (starting points 11 to 71) the velocities in respect to the Prandtl curve are still considerably increased; while at the starting points 12 to 32, farther upstream, this increase has already subsided appreciably. At the points 13 to 23, farthest upstream, it has practically disappeared so that, on the whole, the velocity distribution along the contour decreases substantially with increasing Mach number.

2. Mach Numbers with Divergence of the Computed Flows

The approximate calculation at $M_\infty = 0.80$ and $M_\infty = 0.82$ was carried out by the same scheme and the results plotted in figures 4 and 5. In spite of the much larger number of steps (up to 10),

no satisfactory approximation of the adiabatic curve was obtainable. While at $M_\infty = 0.80$, the ninth and tenth steps appear to approximate the theoretical curve to some small extent, divergence is plainly noticeable at $M_\infty = 0.82$ in the fifth step even as is evident in the starting points 11 and 21. This divergence seems to be traceable to the starting points which extend into the range of supersonic speed ($M^+ > 1$). The significance of the divergence is discussed at the end of the report after the results of approximate calculations for several other profiles are available for the discussion.

3. Discussion of the Computed Maximum Increases of Speed Compared with Busemann's Data

Figure 17 represents the velocities in starting point 11 at various Mach numbers from which the increasing number of necessary steps with increasing M is apparent. When the velocity in starting point 11 nears the velocity of sound, this profile requires about five to six steps by the Prandtl rule to assure sufficiently close approximation. So, while the approximate calculations available so far for slender profiles were, because of the enormous paper work involved, carried out only to the first, in a few cases to the second step by the Prandtl rule, satisfactory compliance with the continuity condition at those high subsonic speeds is definitely not to be counted on. This holds true so much more because by this approximation method the individual steps always yield a little less than by the single-source method because their source yield was not applied in full strength corresponding to the momentary velocity field, but merely in an approximation, the quality of which is equivalent to the degree of approximation of the whole calculation.

From the velocities obtained in the different starting points, the velocity at the point of maximum thickness was then computed by extrapolation with the aid of the tangent condition ($dv = -\frac{v}{r}\,dn$, r = radius of curvature of stream lines), which at the same time represents the maximum velocity occurring at the crescent contour and plotted in figure 19 for the individual approximations in comparison with the values by Prandtl and Busemann. It was found that the first approximation of the single-source method was in good agreement with Busemann's data. Thus, in this example, the arrangement of the single sources was obviously fortunate enough so that the errors of the rough approximation in the zone of maximum increase of speed are nearly obviated. (However, it should be pointed out here that in other cases the agreement is not quite as good as for the crescent, for example, on the ellipse. This defect in the quality of the approximation method is, however, already evidenced during the

calculation in the very nonuniform distribution of the yield of the source along the individual streamlines so that a correction with better distribution of the single sources would have been possible at any time.)

After exceeding the limit of the velocity of sound, figure 19 again indicates that the number of necessary approximation steps increases considerably. A substantially greater number of steps beyond the fifth approximation were calculated and from these the values toward which the velocity tends at starting point 11 for an unlimited number of steps, determined by extrapolation or else, as in the immediate proximity of the point of divergence, by a refined method. It resulted in a very accurately defined limiting Mach number at which the method ceased to converge. The thus obtained point of divergence lies definitely in the supersonic range at a maximum local Mach number of $M^{+}_{max} = 1.096$.

4. Effect of Dissimilar Source Arrangements

The arrangement of the sources must proceed from the point of view of placing the sources so that the areas of high yield of the elementary sources are covered as uniformly as possible with single sources. Particularly, the single sources lying on a stream filament should be distributed for most uniform yield. Since at the start of the approximation, in general, only an incomplete estimation of the stream densities is possible, unfavorable systems of sources may be encountered. Thus, in order to gain an insight into the potential errors introduced, the crescent flow was computed again in the vicinity of the point of divergence with a modified source system, which in figure 16 is contrasted with the old system. In the new system III, the single sources are moved nearer to the area of maximum increase of speed and disposed more closely; owing to this closer coverage near the maximum speed increases, the two outermost sources of system I were omitted so as not to increase the number of sources much above twelve. The results of the approximate calculation [illegible]

below that caused by an insufficient number of approximating steps (as for example, breaking off the calculation after the first or second step beyond the Prandtl rule). Even the fundamental characteristics of the computed flow, such as convergence and divergence of the solutions, remain completely unaffected by the type of special source system.

III. VELOCITY DISTRIBUTION OVER ELLIPSE AND ELONGATED PROFILE ($d/l = 0.10$)

As for the crescent, the compressible flow past an ellipse and a spindle-shaped profile of the same $d/l = 0.10$ was computed and the results for several Mach numbers illustrated in figures 6 to 11. The source system I was used for the spindle-shaped profile while for the ellipse, a different arrangement of sources (system II) was chosen where the single sources extend farther upstream or downstream so as to secure a better adaptation on the more complete velocity distribution of the ellipse. These profiles also evince a point of divergence beyond which the applied calculation method ceases to converge. This point lies at different Mach number of the basic flow, depending upon the particular profile form. But it is always observed when the velocity of sound is locally exceeded in the flow around the profile. This characteristic is especially reproduced for the ellipse in figure 17, where the velocities are compared to several Mach numbers in the immediate proximity of maximum profile thickness (starting point 11).

The maximum increases of speed at the contour $\Delta v_k/v_\infty$ of the ellipse were also computed for the several degrees of approximation and plotted in figure 19 along with the values of Busemann's approximation. At the Mach number of flow corresponding to the divergence point, a local increase of speed of 26.4 percent results, equivalent to a maximum local Mach number of $M^+_{max} = 1.08$. The comparison with Busemann's method of approximation indicates that the first step of the single-source method yields a little more than the corresponding Busemann step. Even though fundamentally the single-source method must yield a little more for the source intensities than Busemann's method, on account of the absent series expansion, the existent difference appears, nevertheless, to be largely attributable to the fact that the chosen system of sources was not well enough adapted to the flow around the ellipse as evidenced by the nonuniform distribution of the yields of the source. However, since the observed difference amounts, at the most, to 0.5 percent of the parallel flow, a correction of the calculation by means of a modified source system was omitted.

IV. VELOCITY DISTRIBUTION ABOUT A CIRCULAR CYLINDER IN COMPARISON WITH LAMLA'S CALCULATIONS

As a further example for calculation by the single-source method, the compressible flow around a circular cylinder was chosen. The Prandtl rule certainly represents no good initial approximation for the flow around a circle, because the assumptions for the applicability of the Prandtl rule, such as regards sufficiently small increases of speed, for example, are not complied with. For this reason, the ordinary incompressible flow was used as the initial approximation for the circle so that the respective sources to be applied must cover the entire stream density difference between the incompressible and the compressible flow. The result of the calculation in the vicinity of the divergence point is reproduced in figures 12 to 15. At $M_\infty = 0.40$, about four steps afford a sufficient approach to the exact adiabatic curve; at $M_\infty = 0.42$, about five steps are already necessary and at $M_\infty = 0.45$, the calculated eight steps indicate that at this Mach number of flow, no convergence can be any longer counted upon; at $M_\infty = 0.50$, divergence definitely prevails. The velocities in the characteristic starting point 11 computed at different Mach numbers clearly show (fig. 18) how the number of necessary approximation steps from 1 to 2 at $M_\infty = 0.25$ up to the divergence point increases considerably and ultimately after exceeding the divergence point, no approximation satisfying the adiabatic equation can be found no matter how many steps are used.

The maximum increases of speed occurring at the circle circumference were computed from the data of the single-source calculation and plotted in figure 20 for different degrees of approximation and Mach numbers. Where the point of divergence lies at around $M_\infty = 0.447$ with a maximum increase of $\Delta v_k/v_\infty = 1.70$, the equivalent to a maximum local Mach number $M^+_{max} = 1.295$. The values of the first to third approximation by Lamla (reference 1) were also included. The comparison indicates good agreement between Lamla's data and those obtained by the single-source method.

V. SIGNIFICANCE OF THE POINT OF DIVERGENCE

In all of the afore-mentioned calculations, it was found that the single-source method, once a certain limiting Mach number had been exceeded, was unable to produce satisfactory approximate solutions because the calculation diverged. Typical for the divergence point was the fact that the highest local Mach number at the profile circumference was only slightly above the sonic velocity. To illustrate: on the

ellipse ($d/l = 0.10$) the highest Mach number related to the divergence point was $M^+_{max} = 1.082$, for the crescent ($d/l = 0.10$) $M^+_{max} = 1.096$, and for the circle, $M^+_{max} = 1.295$. At this state of affairs, the question arises whether perhaps by the rough approximation assumptions of the calculation only the maximum local Mach numbers are shifted into the supersonic range while by the exact calculation the sonic velocity just represents the critical limit at the exceeding of which the convergence stops. On top of that, it is extremely important to decide whether the observed divergence merely represents some defect of the mathematical method of calculation or whether it is perhaps the evidence of a specific physical progress.

To analyze the last problem, the single-source method was modified so that the calculation was reduced to the solution of a 12-term quadratic equation system with 12 unknowns. (This investigation is to be published in a separate report.) After this change, it was possible, for example, to calculate flows past profiles with high local supersonic fields of $M^+_{max} = 1.5$ and more. This therefore proved that the single-source method contains no fundamental difficulty to push ahead into the area of high local supersonic fields. It was also found that above a certain limiting Mach number, equivalent to the divergence point, a solution joining on the subsonic flow no longer exists. Therefore, the reason for the unsatisfactory approximate solution for the compressible flow around circular cylinders, ellipses, and crescent above the point of divergence is due to the fact that above the limiting Mach number, the symmetrical flow pattern postulated by the calculating formula no longer exists, but rather is replaced by an unsymmetrical flow associated with compressibility shocks.

Concerning the maximum local Mach numbers related to the divergence point, it is appropriate to reexamine figures 17 and 18 with the velocity variation in starting point 11. It is seen that the point of divergence is reached when the velocity curve related to this point 11 is exactly tangent to the adiabatic curve. But this contact point is always in the supersonic range as is to be inferred from the ascent of the velocity curve for point 11 and the adiabatic curve. The divergence point could lie then exactly at the sonic velocity only if the velocity curve of point 11 with horizontal tangent approached the adiabatic curve.

The question is then whether the ascent of the velocity curve of point 11 can be varied as far as the horizontal entry in the adiabatic curve by refinement of the calculation formula. The refinement of the formula can, for example, be visualized such that the previously employed 12 single sources are consistently split up until, in the limiting case of the exact calculation, infinitely many small elementary sources are involved; but this splitting up modifies in no way the sum of the yields of the source. Even though this splitting may slightly modify the magnitude of the additional velocities produced by the sources,

that is, shift the total velocity curve from the first approximation somewhat, it is extremely unlikely that the curve up to horizontal entry would be changed as a result. It is therefore necessary to reckon with the fact that the computed local supersonic fields do actually occur and can be symmetrically removed without compressibility shock. By the worked-out model problems, the highest local supersonic Mach numbers still obtained in symmetrical flow are so much greater as the Mach numbers of the airspeeds related to the divergence point are smaller. This is exemplified in figure 21 where the highest local Mach numbers of the divergence point are plotted against the airspeed Mach number for the circle, crescent, and ellipse. At $M_\infty = 1$ the curve of the highest local Mach numbers has the value $M^+_{max} = 1$, hence at this speed the increases of velocity exactly disappear. It means that at sonic velocity $M_\infty = 1$ a symmetrical flow is possible only for the infinitely thin, flat plate in parallel flow which is consistent with the variation of the flow density curve with its maximum at sonic velocity. Figure 21 further shows the Mach numbers of flow at which local sonic velocity is exactly reached. A comparison with the Mach numbers of flow related to the divergence point indicates that both differ very little, the difference becomes less as M_∞ becomes greater. At $M_\infty = 0.80$ the difference amounts to a mere $\Delta M_\infty = 0.030$. So, as far as the application of these data to the conditions in aerotechnics is concerned, it is quite immaterial whether the flow abandons its symmetrical character at the sonic speed limit or at the Mach number of the divergence point and changes to unsymmetrical flow with compressibility shocks. This result holds for the present only for the discussed model flows around the circle, ellipse, and crescent. However, it is not very likely that the conditions will be materially different on other profile forms. Since on the ellipse and on the crescent of equal d/l, for example, profile forms with very dissimilar curvature variation are already involved.

From this point of view, the question of whether the previously computed symmetrical flows with local supersonic flow fields are stable, that is, whether they return to the initial flow attitude after minor disturbances, itself loses importance. In the calculation itself, only the conditions for potential flows, such as continuity, freedom from vortices, etc., were contained so that the problem of stability would have to be treated additionally and therefore it is not ascertainable for the time being.

VI. RESULTS

From the results of the calculations by the method of approximation on compressible plane flows with the aid of single-source arrangements, the following findings were arrived at:

1. The maximum increase of speed on the circumference of a circular cylinder computed by the single-source method and compared with the data by Lamla indicated that the calculated maximum speeds in all comparable degrees of approximation (steps 1 to 3 beyond the incompressible flow) are in very close agreement by both methods.

In the case of the flow around an ellipse, a 0.5-percent difference in airspeed resulted in comparison with Busemann's calculation (approximation step 1), which obviously is attributable to the not very favorable arrangement of the single source. But the magnitude of the error involved did not seem to justify the additional paper work involved in a calculation with an improved source distribution.

The first step for the flow around a crescent beyond the Prandtl rule could be compared with Busemann's calculations; here also the agreement was practically perfect.

The conclusion, therefore, is that the single-source method is suitable for a quick, numerically correct insight into the highest increases of speed accompanying the compressible flow past profiles.

2. As the single-source method affords a clear view of the quality of the attained approximation to the adiabatic curve, it is possible at all times to decide whether the attained degree of approximation of the calculation is already sufficient or whether the number of steps needs to be increased. In this respect, the model problems worked out disclosed that at low airspeeds two to three steps are sufficient, but that in proximity of sonic velocity, six to eight steps are necessary. Thus in this range, the calculations by Rayleigh, Lamla, and Busemann would also have to be continued up to substantially higher degrees if sufficient approximation to the adiabatic curve in the sonic speed range is to be attained.

3. After exceeding a certain Mach number of airspeed, it was no longer possible to secure a satisfactory symmetrical approximate solution with any number of steps because the calculation diverged. Since in other cases it succeeded in computing by the same method subsonic flows with large local supersonic zones ($M^{+}_{max} = \sim 1.5$), the observed divergence cannot be attributed to the imperfect suitability of the employed calculating method. The appearance of the divergence was, therefore, interpreted as that the symmetrical subsonic flow can be continued only up to the Mach number related to the point of divergence and after that, the flow changes into the unsymmetrical type characterized by compressibility shocks.

4. The highest local velocity appearing at the point of divergence lies a little above sonic velocity, the more so the smaller the Mach number of flow related to the point of divergence.

On the circle, for example, the maximum local Mach number is $M^+_{max} = 1.29$, at the crescent $(d/l = 0.10)$ $M^+_{max} = 1.10$, and on the ellipse $(d/l = 0.10)$ $M^+_{max} = 1.08$.

5. The Mach numbers of air flow related to the point of divergence are only a little higher than the Mach numbers of flow at which, locally at the circumference, the sonic velocity is exactly reached for the first time: the difference in Mach number is, for example, $\Delta M_\infty = 0.030$ for the ellipse $(d/l = 0.10)$, $\Delta M_\infty = 0.030$ for the crescent $(d/l = 0.10)$, and $\Delta M_\infty = 0.050$ on the circle. Thus for actual flight practice, it is quite immaterial whether the flow already changes into the unsymmetrical type on reaching sonic speed or at the Mach number of the point of divergence.

6. The flows with local supersonic fields computed by the single-source method satisfy the conditions for potential flows such as continuity, nonturbulence, etc. However, it yet remains to be proved whether the calculated supersonic fields are stable, that is, whether, after a small disturbance, they return in the initial state.

Translated by J. Vanier
National Advisory Committee
for Aeronautics

APPENDIX

METHOD OF CALCULATION

1. Choice of Starting Points and Source Systems

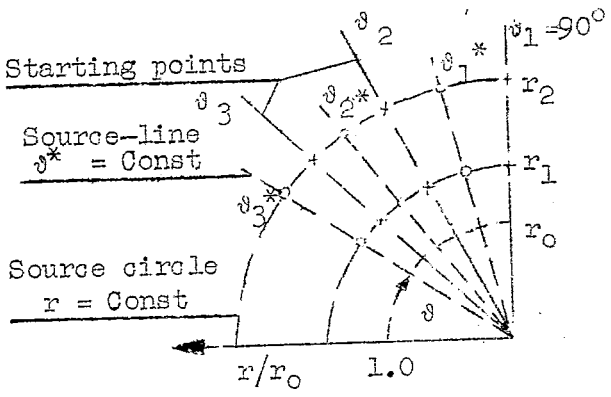

Since the sources to be applied on the crescent and especially at the spindle-shaped body are predominately placed within a comparatively narrow range near the profile center, a system of sources was chosen at which the three-source lines ϑ^* = Constant lie close together (system of points I). For the circular profile and especially for the ellipse on the other hand, the area of the additional sources is more extended toward the stagnation point. Owing to the steep increase of speed at the ellipse aft of the profile nose, the maximum of the additional sources lies for this profile in the forward half of the profile even at high Mach numbers (system of points II). For the study of the influence of the change of the source arrangement, a second system was included for the case of the crescent, where, instead of the 12 sources extending far into the outer space, 13 closely spaced sources were chosen (system III).

Starting Point and Source System I
(Polar Coordinates in the Plane of the Circle)
[Starting point (r_μ, ϑ_ν), Source point $(r_k, \vartheta_\lambda^*)$,
r_o = Radius of image circle]

Starting points ($\mu\nu$) Source points ($k\lambda$)	Starting point and radii of circle of source $r_\mu, k/r_o$ 1.075 1.242 1.436 1.659 2.216 2.959 3.952
Starting point angles ϑ_ν = 90 = 74 = 60	$\mu\nu$ (1 1) (2 1) (3 1) (4 1) (5 1) (6 1) (7 1) (1 2) (2 2) (3 2) (1 3) (2 3)
Source-line angle ϑ^*_λ = 78.75 = 67.5 = 52.5	$k\lambda$ (1 1) (2 1) (3 1) (1 2) (2 2) (3 2) (4 2) (5 2) (6 2) (7 2) (1 3) (2 3)

Starting Point and Source System II

Starting points ($\mu\nu$) Source points ($k\lambda$)	Starting point and radii of circle of source 1.075 1.242 1.436 1.659 2.061 2.572 3.952
Starting-point angles ϑ_ν = 90.0 = 67.5 = 45.0	$\mu\nu$ (1 1) (2 1) (3 1) (4 1) (5 1) (6 1) (7 1) (1 2) (2 2) (3 2) (1 3) (2 3)
Source-line angles ϑ^*_λ = 71.75 = 67.5 = 56.25 = 38.0	$k\lambda$ (1 1) (2 1) (3 1) (4 2) (5 2) (6 2) (7 2) (1 2) (2 2) (3 2) (1 3) (2 3)

Starting Point and Source System III

Starting points ($\mu\nu$) Source points ($k\lambda$)	Starting point and radii of circle of source 1.075 1.242 1.436 1.659 2.061
Starting-point angles ϑ_ν = 90.0 = 78.75 = 67.5	$\mu\nu$(1 1) (2 1) (3 1) (4 1) (5 1) (1 2) (2 2) (3 2) (1 3) (2 3) (3 3) (4 3) (5 3)
Source-line angles ϑ^*_λ = 84.35 = 73.12 = 61.88	$k\lambda$ (1 1) (2 1) (3 1) (1 2) (2 2) (3 2) (4 2) (5 2) (1 3) (2 3) (3 3) (4 3) (5 3)

2. Influence Factors in the Cyclic (circular) Plane

With $\underline{x}^* = Re^{i\vartheta^*}$ denoting the local vector of a source and $\underline{x} = re^{i\vartheta}$ the starting point, the velocity induced in the starting point is

[1]Throughout this report $\underline{x}$ and $\underline{y}$ are substituted for the German script x and v which were used in the original German version.

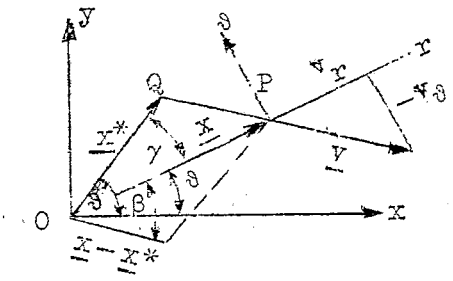

$$\frac{\underline{v}}{\vartheta_\infty} = \frac{\tilde{E}}{2\pi} \frac{r_o}{R} \frac{R^2}{r^2} \frac{\underline{x} - \underline{x}^*}{R}$$

when $\tilde{E} = \frac{E}{r_o V_\infty}$ represents the source strength and

$$\frac{r'}{R} = \sqrt{1 + \left(\frac{r}{R}\right)^2 - 2\frac{r}{R} \cos(\vartheta^* - \vartheta)}$$

the spacing. If the system of the coordinates is rotated through ϑ, radial and tangential components in the starting points change into the x and y components of the new system. Thus, with $r/R = \tau$, $\vartheta^* - \vartheta = \gamma$

$$\frac{\underline{v}}{v_\infty} e^{-i\vartheta} = \frac{vr + iv\vartheta}{v_\infty}$$

$$= \frac{\tilde{E}}{2\pi} \frac{r_o}{R} \frac{(\tau - \cos\gamma) - i \sin\gamma}{1 + \tau^2 - 2\tau \cos\gamma}$$

hence for the ϑ components

$$\frac{v_\vartheta}{v_\infty} = \frac{\tilde{E}}{2\pi} \frac{r_o}{R} f_{v_\vartheta}$$

with

$$f_{v_\vartheta} = \frac{-\sin\gamma}{\sin^2\gamma + (\tau - \cos\gamma)^2}$$

The contour conditions are satisfied by adding to each principal source (Hqu) the source (Spqu) reflected at the contour circle. If the source arrangement is in addition doubly symmetrical, that is, sources of equal strength in $\pm\vartheta^*$ sources and in $\pm(\pi - \vartheta^*)$ sources, four principal sources each can be combined. For $\gamma = (\vartheta^* - \vartheta)$ and $\gamma = -(\vartheta^* + \vartheta)$, $f_{v\vartheta}$ is to be assumed positive, for $\gamma = \pi - (\vartheta^* - \vartheta)$ and $\gamma = -\pi + (\vartheta^* - \vartheta)$, negative, so that

$$\sum_4 f_{v\vartheta} = \left\{ \frac{\sin(\vartheta^* + \vartheta)}{\sin^2(\vartheta^* + \vartheta) + \left[\tau - \cos(\vartheta^* + \vartheta)\right]^2} + \frac{\sin(\vartheta^* + \vartheta)}{\sin^2(\vartheta^* + \vartheta) + \left[\tau + \cos(\vartheta^* + \vartheta)\right]^2} \right\} - \left\{ \frac{\sin(\vartheta^* - \vartheta)}{\sin^2(\vartheta^* - \vartheta) + \left[\tau - \cos(\vartheta^* - \vartheta)\right]^2} + \frac{\sin(\vartheta^* - \vartheta)}{\sin^2(\vartheta^* - \vartheta) + \left[\tau + \cos(\vartheta^* - \vartheta)\right]^2} \right\} \quad (1)$$

In order to better assess the influence of a continuous source distribution by a system of 12 single sources, the latter are visualized as being replaced by a source-line system with two-dimensional source strength distributed along rays $\vartheta^* = \text{Constant}$. Combining then the influence of one radius at the source points by averaging and taking the source strength along the interval as constant, the influence of a step-like source distribution along the ray $\vartheta^* = \text{Constant}$ that substitutes the line superposition is closely approximated although in the practical calculation only single sources are involved. Unless the influence quantity $\sum_4 f_{v\vartheta}$ plotted for fixed ϑ and fixed ϑ^* against τ varies excessively, the mean influence is equal to the influence in the center, or within the framework of the distribution by powers of 1.075 in the intermediate partial points. In the vicinity of the extremes of the influence curves at $\tau = 1$, however, and at interval increases at the fourth source ring the average value of the interval must be computed more accurately. Indicating the average formation by overscoring and including the factor $1/2\pi$ in the influence factor, the final ϑ component of the induced velocity follows as

$$\frac{v_\vartheta}{v_\infty} = \tilde{E} f_{\vartheta^*} \quad \text{with} \quad f_{\vartheta^*} = \frac{1}{2\pi}\left[\left(\frac{r_o}{R}\sum_4 f_{v\vartheta}\right)_{Hqu} + \left(\frac{r_o}{R}\overline{\sum_4 f_{v\vartheta}}\right)_{spqu}\right] \quad (2)$$

3. Conformal Transformation and the Ensuing Velocity Distortion

The conformal transformation $Z_{ik}^* = f(\zeta)$ gives the flow around the profile in the ik^* plane from the flow around the image circle $|\zeta| = r_o$. The complex potential $\chi = \varphi + i\psi$ is

$$\left(\frac{v}{v_\infty}e^{-i\alpha}\right)_{ik}^* = \frac{d\chi}{dZ_{ik}^*} = \frac{d\chi}{d\zeta}\,\frac{d\zeta}{dZ_{ik}^*} = \frac{v/v_\infty}{F}e^{-i(\epsilon+\alpha)}$$

and the distortion function $\frac{dZ_{ik}^*}{d\zeta} = Fe^{i\epsilon}$ is

$$F = \frac{(v/v_\infty)_{circle}}{(v/v_\infty)_{ik}^*} \qquad \epsilon = \alpha_{ik}^* - \alpha_{circle}$$

The flow around the circle $|\zeta| = r_o$ as contour is with $\zeta = re^{i\vartheta}$ and $\chi = \zeta + \frac{r_o}{\zeta}$

$$\frac{v}{v_\infty}e^{-i\alpha} = \frac{v_x - iv_y}{v_\infty} = \frac{d\chi}{d\zeta} = 1 - \frac{r_o^2}{\zeta^2} = \left[1 - \left(\frac{r_o}{r}\right)^2 \cos 2\vartheta\right] + i\left(\frac{r_o}{r}\right)^2 \sin 2\vartheta$$

and

$$\frac{v}{v_\infty} = \sqrt{1 + \left(\frac{r_o}{r}\right)^4 - 2\left(\frac{r_o}{r}\right)^8 \cos 2\vartheta} \quad \begin{array}{l} \xrightarrow[\vartheta = \frac{\pi}{2}]{} 1 + (r_o/r)^2 \\ \xrightarrow[r = r_o]{} 2 \sin \vartheta \end{array} \qquad (3)$$

To determine then the velocity of a specific profile in the ik^*-plane, only the distortion needs to be computed.

a. Crescent.- If δ is the edge angle of the crescent and

$$(d/l)_{ik}^* = 0.10/\mu \qquad \left(\mu = \frac{1}{\sqrt{1 - M_\infty^2}} = \text{Prandtl factor}\right)$$

the thickness ratio of the given comparative profile, the geometry of the crescent gives

$$\tan\frac{\delta}{4} = \left(\frac{d}{\ell}\right)^*_{ik}$$

The conformal transformation is attained by

$$\frac{\frac{Z_{ik}^*}{r_o} - n}{\frac{Z_{ik}^*}{r_o} + n} = \left(\frac{\frac{\zeta}{r_o} - 1}{\frac{\zeta}{r_o} + 1}\right)^n$$

or

$$\frac{Z_{ik}^*}{r_o} = n\,\frac{\left(1 - S^{2n}\right) + i\left(2S^n \sin n\beta\right)}{1 + S^{2n} - 2S^n \cos n\beta}$$

with

$$Se^{i\beta} = \frac{\frac{\zeta}{r_o} - 1}{\frac{\zeta}{r_o} + 1}$$

The quantities S and β can be represented as functions of the circular coordinates

$$S^2 = \frac{\left(\frac{r}{r_o}\right)^2 + 1 - 2\frac{r}{r_o}\cos\vartheta}{\left(\frac{r}{r_o}\right)^2 + 1 + 2\frac{r}{r_o}\cos\vartheta} \xrightarrow{\vartheta = \pi/2} 1 \qquad \xrightarrow{r = r_o} \tan^2(\vartheta/2)$$

$$\beta = \frac{\operatorname{arc\,tan}\, 2\frac{r}{r_o}\sin\vartheta}{\left(\frac{r}{r_o}\right)^2 - 1} \xrightarrow{\vartheta = \pi/2} \operatorname{arc\,tan}\frac{2r/r_o}{\left(r/r_o\right)^2 - 1} \qquad \xrightarrow{r = r_o} \pi/2$$

The profile parameter n is given by the thickness ratio. As exponent it indicates the multiplication of the angle π in the stagnation point of the circle. It is

$$\pi n = 2\pi - \delta$$

or

$$n = 2 - \frac{4}{\pi} \operatorname{arc\,tan}\left(\frac{d}{l}\right)^*_{ik}$$

The velocity distortion follows from

$$\frac{dZ_{ik}}{d\zeta}^* = Fe^{i\epsilon} = \frac{\left(Se^{i\beta}\right)^{\frac{1}{2}} - \left(Se^{i\beta}\right)^{-\frac{1}{2}}}{\left(Se^{i\beta}\right)^{\frac{n}{2}} - \left(Se^{i\beta}\right)^{-\frac{n}{2}}}$$

as

$$F = n^2 \frac{S + \left(\frac{1}{S}\right) - 2\cos\beta}{S^n + \left(\frac{1}{S^n}\right) - 2\cos n\beta}$$

(4)

$$\epsilon = 2 \operatorname{arc\,tan}\left(\frac{S+1}{S-1}\tan\frac{\beta}{2}\right) - 2 \operatorname{arc\,tan}\left(\frac{S^n+1}{S^n-1}\tan\frac{n\beta}{2}\right)$$

The formula of the conformal transformation was so chosen that parallel flow prevails at infinity. Actually it is

$$\frac{dZ_{ik}}{d\zeta}^* \xrightarrow[S = 1,\ \beta = 0]{} n^2\frac{\sin^2\frac{\beta}{2}}{\sin^2 n\frac{\beta}{2}} \longrightarrow 1$$

which conditions that $\frac{l/2}{r_o} = n$.

b. Elongated body of revolution. — The conformal transformation is supplied by the formula satisfying $\frac{dZ_{ik}^*}{d\zeta} \xrightarrow[\infty]{} 1$

$$\frac{Z_{ik}^*}{r_o} = \frac{\zeta}{r_o} + K\frac{r_o}{\zeta} + \frac{1 - K}{3}\left(\frac{r_o}{\zeta}\right)^3$$

$$= \left[\left(\frac{r}{r_o} + \frac{K}{r/r_o}\right)\cos\vartheta + \frac{1 - K}{3}\left(\frac{r_o}{r}\right)^3 \cos 3\vartheta\right]$$

$$+ i\left[\left(\frac{r}{r_o} - \frac{K}{r/r_o}\right)\sin\vartheta - \frac{1 - K}{3}\left(\frac{r_o}{r}\right)^3 \sin 3\vartheta\right]$$

Since $\frac{l/2}{r_o} = 2\frac{2 + K}{3}$ and $\left(\frac{d/2}{r_o}\right)_{ik}^* = 2\frac{2(1 - K)}{3}$ is obtained, the profile parameter K is

$$K = \frac{2\left[1 - \left(\frac{d}{l}\right)_{ik}^*\right]}{2 + \left(\frac{d}{l}\right)_{ik}^*}$$

and

$$\frac{1 - K}{3} = \frac{\left(\frac{d}{l}\right)_{ik}^*}{2 + \left(\frac{d}{l}\right)_{ik}^*}$$

The velocity distortion follows from the ik* - velocity at

$$\left(\frac{v_x - iv_y}{v_\infty}\right)_{ik}^* = \frac{1 - \left(\frac{r_o}{\zeta}\right)^2}{\left[1 - \left(\frac{r_o}{\zeta}\right)^2\right]\left[1 + (1 - K)\left(\frac{r_o}{\zeta}\right)^2\right]}$$

With

$$N = \left(\frac{r}{r_o}\right)^4 + 2\left(\frac{r}{r_o}\right)^2 (1 - K) \cos 2\vartheta + (1 - K)^2$$

we get

$$\left(\frac{v_x - iv_y}{v_\infty}\right)^*_{ik} = \frac{1}{N}\left(\frac{r}{r_o}\right)^2 \left\{\left[\left(\frac{r}{r_o}\right)^2 + (1 + K) \cos 2\vartheta\right] + i\left[(1 - K) \sin 2\vartheta\right]\right\}$$

and

$$\left(\frac{v}{v_\infty}\right)^*_{ik} = \frac{(r/r_o)^2}{\sqrt{N}}$$

hence, with (3)

$$F^2 = \left[1 + \left(\frac{r_o}{r}\right)^4 (1 - K)^2 + 2\left(\frac{r_o}{r}\right)^2 (1 - K) \cos 2\vartheta\right] \left[1 + \left(\frac{r_o}{r}\right)^4 - 2\left(\frac{r_o}{r}\right)^2 \cos 2\vartheta\right]$$

$$= A + B \cos 2\vartheta + C \cos 4\vartheta$$

where

$$\begin{aligned} A &= 1 + K^2\left(\frac{r_o}{r}\right)^4 + (1 - K)^2\left(\frac{r_o}{r}\right)^8 \\ B &= 2K\left(\frac{r_o}{r}\right)^2 \left[(1 - K)\left(\frac{r_o}{r}\right)^4 - 1\right] \\ C &= -2(1 - K)\left(\frac{r_o}{r}\right)^4 \end{aligned} \tag{5}$$

c. Ellipse.— A corresponding formula supplies the conformal transformation:

$$\frac{Z_{ik}^*}{r_o} = \frac{\zeta}{r_o} + \frac{a^2}{r_o^2}\frac{r_o}{\zeta}$$

$$= \frac{r}{r_o}\left[\left(1 + \frac{a^2}{r^2}\right)\cos\vartheta + i\left(n - \frac{a^2}{r^2}\right)\sin\vartheta\right]$$

with

$$\frac{a^2}{r_o^2} = \frac{1 - \left(\frac{d}{l}\right)_{ik}^*}{1 + \left(\frac{d}{l}\right)_{ik}^*}$$

as profile parameter. The velocity distortion follows from

$$\frac{dZ_{ik}^*}{d\zeta} = \left(1 - \frac{a^2}{\zeta^2}\right)$$

$$= \left(1 - \frac{a^2}{r^2}\cos 2\vartheta\right) + i\left(\frac{a^2}{r^2}\sin 2\vartheta\right)$$

as

$$F = \sqrt{1 + \left(\frac{a}{r}\right)^4 - 2\left(\frac{a}{r}\right)^2\cos 2\vartheta}$$

$$\tan\epsilon = \frac{\left(\frac{a}{r}\right)^2\sin 2\vartheta}{1 - \left(\frac{a}{r}\right)^2\sin 2\vartheta} \qquad (6)$$

hence, with (3) the velocity becomes

$$\frac{v_{ik}^*}{v_\infty} = \sqrt{\frac{1 + \left(\frac{r_o}{r}\right)^4 - 2\left(\frac{r_o}{r}\right)^2 \cos 2\vartheta}{1 + \left(\frac{a}{r}\right)^4 - 2\left(\frac{a}{r}\right)^2 \cos 2\vartheta}} \xrightarrow{\vartheta = \pi/2} \frac{1 + (r_o/r)^2}{1 + (a/r)^2} = \frac{1 + (d/l)_{ik}^*}{1 + (d/l)_{ik}^* \frac{1 - (r_o/r)^2}{1 + (r_o/r)^2}}$$

$$\xrightarrow{r = r_o} \frac{2 \sin \vartheta}{\sqrt{1 + (a/r_o)^4 - 2(a/r_o)^2 \cos 2\vartheta}}$$

$$= \left[1 + \left(\frac{d}{l}\right)_{ik}^*\right] \frac{\sin \vartheta}{\sqrt{\sin^2 \vartheta + \left(\frac{d}{l}\right)_{ik}^{*2} \cos^2 \vartheta}}$$

4. Determination of Source Strength for Assessing the Difference Between the Exact Stream Density and the Employed Approximation

If $\theta_k = \frac{\rho_k v_k}{\rho^x a^x}$ is the stream density of the compressible flow, we get with $M_k^* = \frac{v_k}{a^*}$, $M_\infty = \frac{v_\infty}{a_\infty}$ (a = local sonic velocity, a^x = critical velocity of sound) as a result of the adiabatic phase change

$$\frac{\theta_k}{\theta_\infty} = \frac{M_k^*}{M_\infty^*} \left[1 - \frac{\kappa - 1}{2} M_\infty^2 \left(\frac{M_k^{*2}}{M_\infty^{*2}} - 1\right)\right]^{\frac{1}{\kappa - 1}} \tag{7}$$

with $\kappa = \frac{c_p}{c_v} = 1.405$. Considering only the linear terms in the interference velocity conformably to Prandtl and putting

$$\frac{M_k^*}{M_\infty^*} = 1 + \frac{\Delta M_k^*}{M_\infty^*}$$

gives with

$$1 - M_\infty^2 = \frac{1}{\mu^2}$$

$$\frac{\theta_k}{\theta_k} \approx \left(1 + \frac{\Delta M_k^*}{M_\infty^*}\right)\left(1 - M_\infty^2 \frac{\Delta M_k^*}{M_\infty^*}\right) \approx 1 + \frac{1}{\mu^2}\frac{\Delta M_k^*}{M_\infty^*} = A\frac{M_k^*}{M_\infty^*} + B$$

with

$$A = \frac{1}{\mu^2}, \quad B = M_\infty^2$$

yielding

$$\frac{\theta_{Pr}}{\theta_\infty} = 1 + \frac{1}{\mu^2}\left(\frac{M_k^*}{M_\infty^*} - 1\right) \tag{8}$$

as linearized Prandtl-stream density.

Differentiation of (7) gives as slope of the stream density curve at point M_∞^*

$$\frac{\frac{d\theta_k}{\theta_\infty}}{\frac{dM_k^*}{M_\infty^*}} = \left(1 - M_k^2\right)\frac{\theta_k}{\theta_\infty}\frac{M_\infty^*}{M_k^*} \xrightarrow{M_k^* = M_\infty^*} \frac{1}{\mu^2}$$

The Prandtl-stream density θ_{Pr}, therefore, represents the tangent to the stream density curve in the approach flow point, while the incompressible stream density at speed M_k^*

$$\frac{\theta_{ik}}{\theta_\infty} = \frac{M_k^*}{M_\infty^*} = 1 + \frac{\Delta M_k^*}{M_\infty^*} \tag{9}$$

can be regarded as secant through the points $M_k^* = 0$ and $M_k^* = M_\infty^*$.

Now in order to be able to secure an improved solution for the compressible flow with the aid of the approximated stream density $\theta_N = \theta_{Pr}$ or θ_{ik}, respectively, the compressible flow in a flow tube is visualized as being replaced by a flow of approximated stream density θ_N with identical velocity field, in which the additional displacement is produced by an additional source distribution. (Compare UM 1117, p. 3). If dn_k is the width of the flow tube at a given point,

$$d\tilde{\Psi}_k = \frac{d\Psi_k}{r_o v_\infty} = \frac{dn_k}{r_o}\frac{\theta_k}{\theta_\infty}$$

will be valid for the flow along the flow tube. The approximation flow with additional sources is to show the same velocities as the compressible flow. Due to the source distribution, the flow then differs from point to point:

$$d\tilde{\Psi}_N = \frac{d\Psi_N}{r_o v_\infty} = \frac{dn_N}{r_o}\frac{\theta_N}{\theta_\infty}$$

Both θ_k and θ_N are functions of the velocity M_k^*/M_∞^*. At infinity, the flow is the same in both cases, due to $\theta_{N_\infty} = \theta_\infty$. The sum of all volume sources to be placed upstream then is (compare UM 1117, p. 28)

$$d\tilde{E}_N = \sum \frac{E}{v_\infty r_o} = d\tilde{\Psi}_N - d\tilde{\Psi}_{N_\infty} = \frac{dn_k}{r_o}\left(\frac{\theta_N - \theta_k}{\theta_\infty}\right)$$

If one introduces the constant flow $d\psi_k$, which is calculated, say, in the center section of the doubly-symmetrical profile,

$$d\tilde{E}_N = C_N^*\left(\frac{dn_k}{r_o}\frac{\theta_k}{\theta_\infty}\right)_{\text{center section}} \text{ with } C_N^*\left(\frac{M_k^*}{M_\infty^*}\right) = \frac{\theta_N - \theta_k}{\theta_k} \qquad (10)$$

is valid. C_N^* denotes, therefore, the relative error of the approximated stream density in contrast to the exact stream density for the compressible velocity M_k^*.

a. Incompressible basic flow (flow around circular profile).- The curve of the source strength to be disposed about the circular profile in the incompressible flow is, therefore

$$d\tilde{E}_{ik} = C_{ik}^*\left(\frac{dn_k}{r_o}\frac{\theta_k}{\theta_\infty}\right)_{\text{center section}} \text{ with } C_{ik}^* = \frac{\theta_{ik} - \theta_k}{\theta_k} \qquad (10')$$

The width of the flow tubes at the circle in the center section is

$$\left(\frac{dn_k}{r_o}\right)_{\text{center section}} = \frac{dy_k}{r_o} = \frac{dr}{r_o}$$

b. Prandtl basic flow (crescent, spindle-shaped body, ellipse).- For their profiles the Prandtl approximation is considered as comparative flow and the profile analyzed in the affinely distorted ik*-plane instead of in the compressible plane. With M_{ik^*o} denoting the velocity at the profile of the ik*-plane, as it is attained from the cyclic flow free from sources by conformal transformation, the velocity of the Prandtl approximation M_{k^*o} on the profile of the k-plane obtained by the transformation

$$\frac{M_{k^*o}}{M_{\infty^*}} = 1 + \mu^2 \left(\frac{M_{ik^*o}}{M_{\infty^*}} - 1 \right) \tag{11}$$

corresponding to the linearization of the stream density in (8). The related stream density, therefore, is

$$\frac{\theta_{Pro}}{\theta_\infty} = 1 + \frac{1}{\mu^2} \left(\frac{M_{k^*o}}{M_{\infty^*}} - 1 \right) = \frac{M_{ik^*o}}{M_{\infty^*}}$$

with $\frac{\theta_{ik^*}}{\theta_\infty} \frac{M_{ik^*}}{M_\infty}$ denoting the incompressible stream density related to M_{k^*o} in the ik*-plane, the transformation of the stream density follows as

$$\theta_{Pr} = \theta_{ik^*} \tag{12}$$

Now, if the Prandtl flow M_{k^*o} in the compressible plane corresponds to the flow M_{ik^*o} in the ik*-plane, the Prandtl flow M_{k^*} provided with additional sources replacing the compressible flow corresponds to a flow in the ik*-plane fitted with sources, the velocity of which is equal to the velocity M_{ik^*} transformed by (11)

$$\frac{M_{ik^*}}{M_{\infty^*}} = 1 + \frac{1}{\mu^2} \left(\frac{M_{k^*}}{M_{\infty^*}} - 1 \right)$$

The throughflow of the M_{ik^*} - flow with sources at a point of flow, tube width dn_{ik^*}, is then, since by (12) $\theta_{ik^*} - \theta_{Pr}$ Prandtl is the related stream density,

$$d\tilde{\psi}_{ik^*} = \frac{dn_{ik^*}}{r_o} \frac{\theta_{Pr}}{\theta_\infty}$$

Owing to the source distribution this throughflow varies from one place to another. An infinite distance $d\psi_{ik}{}^*_\infty = \frac{dn_{ik}{}^*_\infty}{r_o}$ hence, the sum of the source strengths in the ik*-plane

$$d\tilde{E}_{ik}{}^* = \frac{dn_{ik}{}^*}{r_o}\left(\frac{\theta_{Pr}}{\theta_\infty} - \frac{dn_{ik}{}^*_\infty}{dn_{ik}{}^*}\right)$$

For their profiles, however, $\frac{dn_{ik}{}^*_\infty}{dn_{ik}{}^*} = \frac{dn_{k\infty}}{dn_k}$ and in the corresponding compressible flow $dn_k\theta_k = dn_{k_\infty}\theta_\infty$ by reason of the continuity. Therefore, the source strength to be applied in the ik*-plane is

$$d\tilde{E}_{ik}{}^* = \frac{dn_{ik}{}^*}{r_o}\left(\frac{\theta_{Pr} - \theta_k}{\theta_\infty}\right) = C_{Pr}{}^*\left(\frac{dn_{ik}{}^*}{r_o}\frac{\theta_k}{\theta_\infty}\right) \text{ with } C_{Pr}{}^* = \frac{\theta_{Pr} - \theta_k}{\theta_k} \quad (10'')$$

while by (10) the k-plane follows at

$$d\tilde{E}_k{}^* = C_{Pr}{}^*\left(\frac{dn_k}{r_o}\frac{\theta_k}{\theta_\infty}\right) = \mu\, d\tilde{E}_{ik}{}^*$$

The source strength per width of flow tube remains, therefore, unchanged by the transformation. On comparing (10'') with (10') it is seen that, owing to (12), the same source strength $d\tilde{E}_{ik}{}^*$ had to be placed in the ik*-plane, if a compressible flow was to be computed by means of additive sources, which is to flow through the flow tube of the ik*-plane and there attain the velocity $M_{ik}{}^*$ of the incompressible flow with sources.

5. Iteration Process

Since in the formula for computing the source strength the unknown compressible velocity $M_k{}^*$ enters on the righthand side of (10), the source strength must be calculated step by step. With $(M_k{}^*{}_o)_{\mu\nu}$ as the velocity in the starting point $\mu\nu$ of the comparative flow used as basis, that is, of the incompressible circular flow or Prandtl flow around one of the thin profiles the relative error of the related approximation stream density $\theta_N(M_k{}^*{}_o)$ in respect to the actual stream density $\theta(M_k{}^*{}_o)$ is computed at the points $(M_k{}^*{}_o)_{\mu\nu}$ after which (10) affords a first approximation for the looked for source

sum $\sum \frac{E}{r_o v_\infty} = \sum_\lambda \tilde{E}_{k\lambda}$. Generally, if $\left(M_k^{*(n-1)}\right)_{\mu\nu}$ are the velocities of the (n-1)th approximation, the source strength sum of nth approximation is

$$\left[\sum_\lambda \tilde{E}_{k\lambda}^{(n)}\right]_{\mu\nu} = a_\mu^{(n-1)}\left[\frac{\theta_N^{(n-1)}}{\theta_k\, M_k^{*(n-1)}} - 1\right] \qquad (13)$$

with

$$a_\mu^{(n-1)} = A_\mu\left[\frac{\theta_k\, M_k^{*(n-1)}}{\theta_\infty}\right]_\mu$$

where $\theta_k\left(M_k^{*(n-1)}\right)$ is preferably taken from a diagram,[1] and A_μ represents the width of the stream tube in midsection. It is $A_\mu = \frac{\Delta r}{r_o}$ and $\left(\frac{\Delta y_{ik}^*}{r_o}\right)_\vartheta = \frac{\pi}{2}$ respectively. Since the outermost source ring must include all the sources existing in the outer space, we get, for example, for the residual source ring $\frac{R_7}{r_o} = 3.952$, if $\frac{R_7}{r_o} = 3.298$ represents the limiting ring of the influence ring $\left(\frac{\Delta r}{r_o}\right)_6$ related to $\frac{r_6}{r_o}$.

$$A_7 = \left[\frac{y_{ik}^*}{r_o}(r_7) - \frac{y_{ik}^*}{r_o}(R_7)\right] + 0.38\,\frac{y_{ik}^*}{r_o}(r_7)$$

$$= 1.38\,\frac{y_{ik}^*}{r_o}(r_7) - \frac{y_{ik}^*}{r_o}(R_7)$$

where 0.38 indicates a reduction factor for the influence of the outer space. The individual source strengths $E_{k\lambda}^{(n)}$ follow then from the difference of two source sums in adjacent points on the same ring, since they relate to the same flow tubes. The additive velocities $\Delta M_k^{*(n)}$ of nth approximation induced by the sources $\tilde{E}_{k\lambda}^{(n)}$ in the starting points $\mu\nu$ are obtained by means of the influence factors f_θ^* at the circle, by neglecting the r-component and taking the ϑ-component equal to the total velocity. (Compare UM 1117, p. 3.)

[1]For thin profiles for which the velocity differs little from the approved flow, the exact stream density curve (7) can, in vicinity of sonic velocity, be closely approximated by a parabola, (compare Oswatitsch). On expanding the bracket in power of $\Delta M_k^* = M_k^* - 1$ and discounting all but the squared terms, we get $\theta_k \approx 1 - \frac{k+1}{2}\left(1 - M_k^*\right)^2$.

The influence factors for the velocity $\left(\frac{\Delta v}{v_\infty}\right)_{\mu\nu}$ of the source $\kappa\lambda$ of the circular flow are, because of (2) simply

$$f_{\kappa\lambda}^{\mu\nu} = f_\vartheta *$$

The total effect of all sources in the starting point $\mu\nu$ is obtained then by summation over all sources $\kappa\lambda$

$$\left[\Delta M_k *^{(n)}\right]_{\mu\nu} = \sum_{\kappa\lambda} M_\infty * f_{\kappa\lambda}^{\mu\nu} \tilde{E}_{\kappa\lambda}^{(n)} \qquad (14)$$

For the profile flow the influence factors (2) must be, in correspondence with the conformal transformation, divided by the distortion quantities (4, 5, 6):

$$f_{\kappa\lambda}^{\mu\nu} = \frac{f_\vartheta *}{F_{\mu\nu}}$$

and the additive velocities according to Prandtl distorted corresponding to (11)

$$\left[\Delta M_k *^{(n)}\right]_{\mu\nu} = \mu^2 M_\infty * \sum_{\kappa\lambda} f_{\kappa\lambda}^{\mu\nu} \tilde{E}_{\kappa\lambda}^{(n)} \qquad (14)$$

with this velocity connection the total velocities of the nth approximation are:

$$M_k *^{(n)} = M_k *_o + \Delta M_k *^{(n)} \qquad (15)$$

If to the initial velocity $M_k *_o$ there corresponds the stream density of the basic comparative flow $\theta_k^{(o)} = \theta_{ik}\left(M_k *_o\right)$ or $\theta_{Pr}\left(M_k *_o\right)$, respectively, then to the improved velocity $M_k *^{(n)}$ there pertains already a stream density nearer to the correct θ-curve; $\theta_k^{(n)}$ is calculated from (13) by solution of the equation with respect to θ_k, and by substituting for all magnitudes on the right side the values that correspond to the new approximation

$$\theta_k(n) = \frac{\theta_N\left[M_k^*(n)\right]}{1 + \frac{\Sigma_\lambda \tilde{E}_{*\lambda}(n)}{a_\mu(n)}}$$

with

$$a_\mu(n) = A_\mu\left[\theta_k \frac{M_k^*(n)}{\theta_\infty}\right]_\mu \tag{16}$$

Connecting the points $M_k^*(n)$, $\theta_k(n)$ for each starting point gives a set of curves which at convergence of the method approach the θ-curve consistently. The points of equal approximation give a picture of the already attained approximation of the θ-curve.

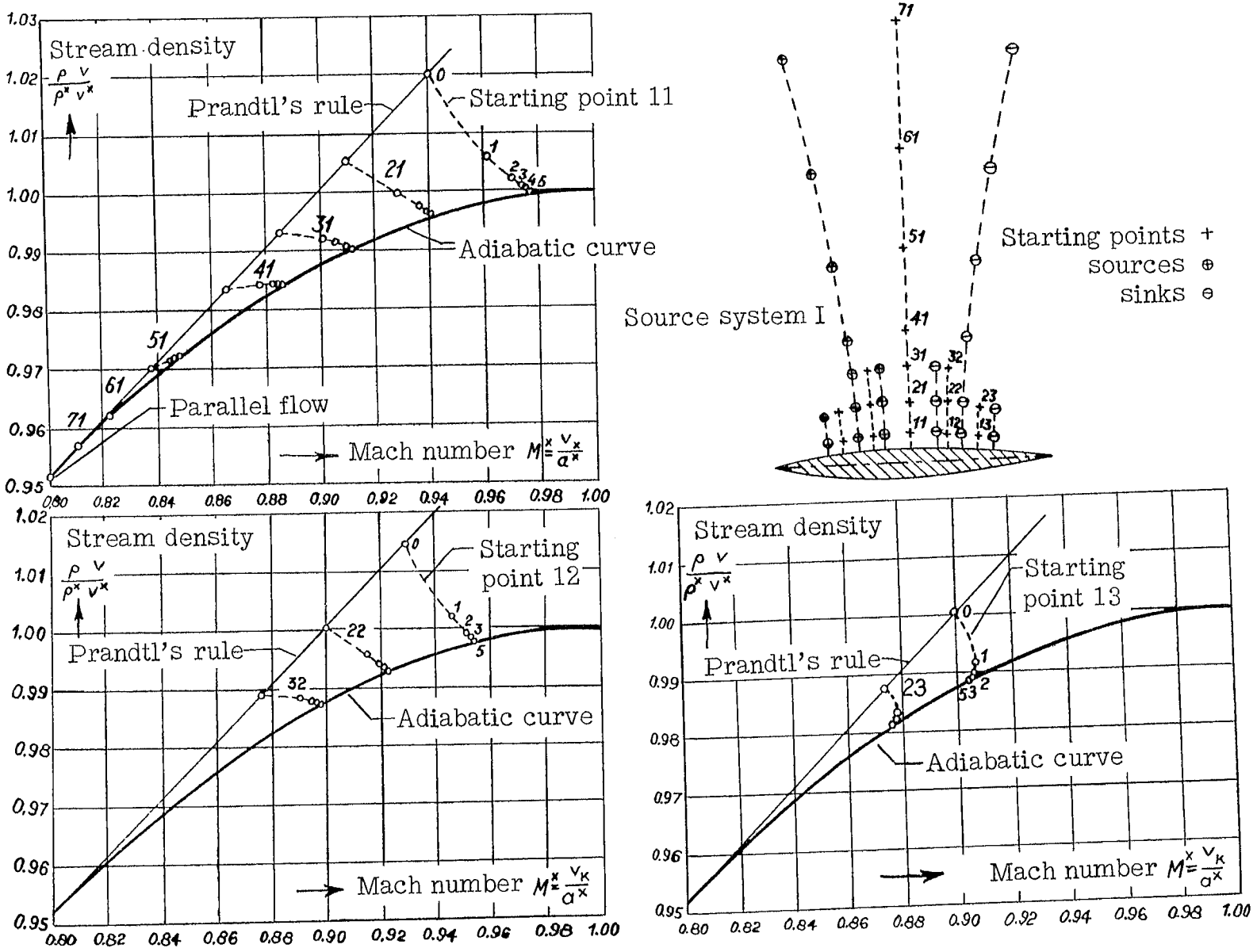

Figure 1.- Line (crescent) ($d/l = 0.10$), $M_\infty = 0.77$.
Velocity and stream density for various approximations to the adiabatic curve (source system I).

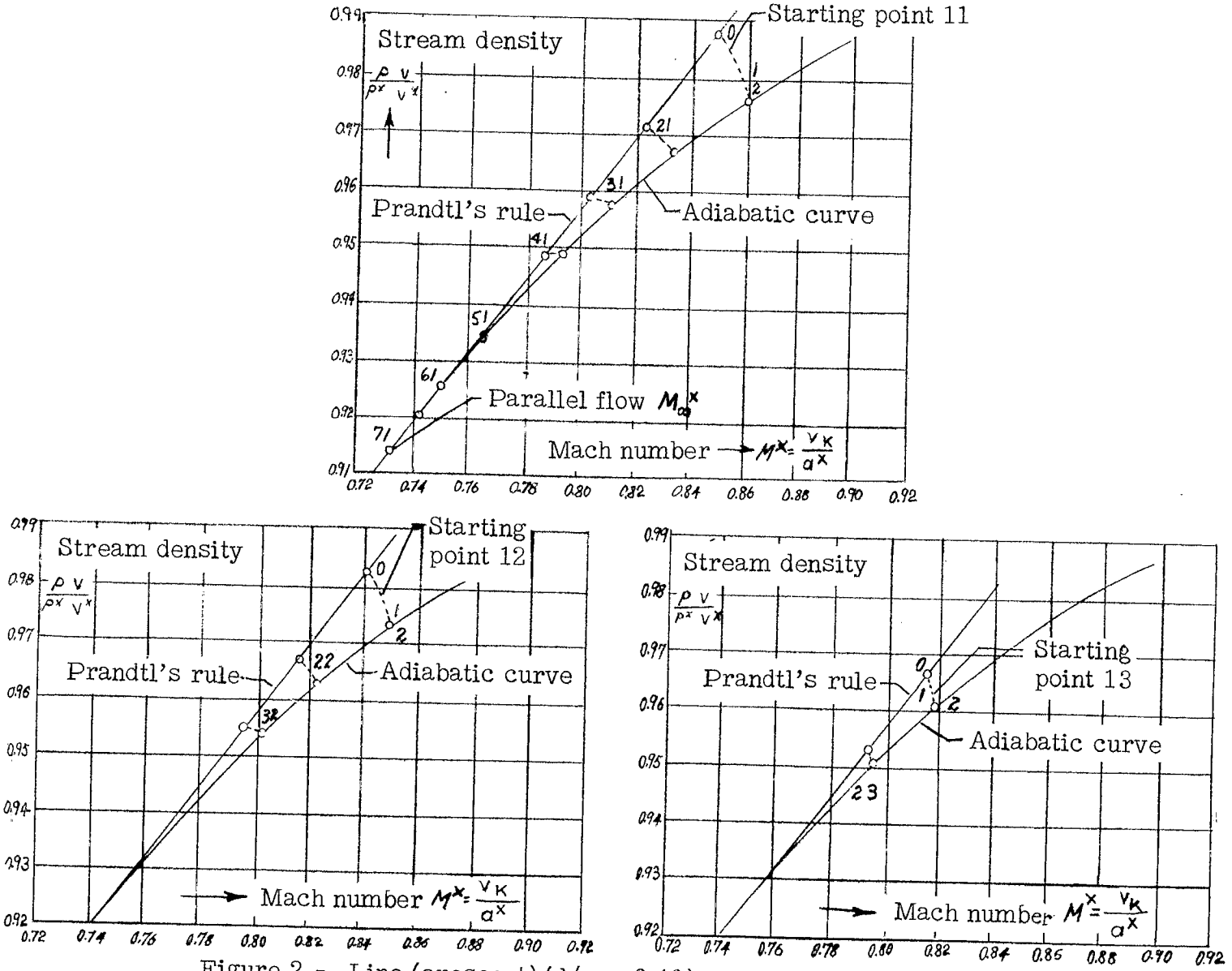

Figure 2.- Line (crescent) ($d/l = 0.10$), $M_\infty = 0.70$. Velocity and stream density for various approximations to the adiabatic curve (source system I).

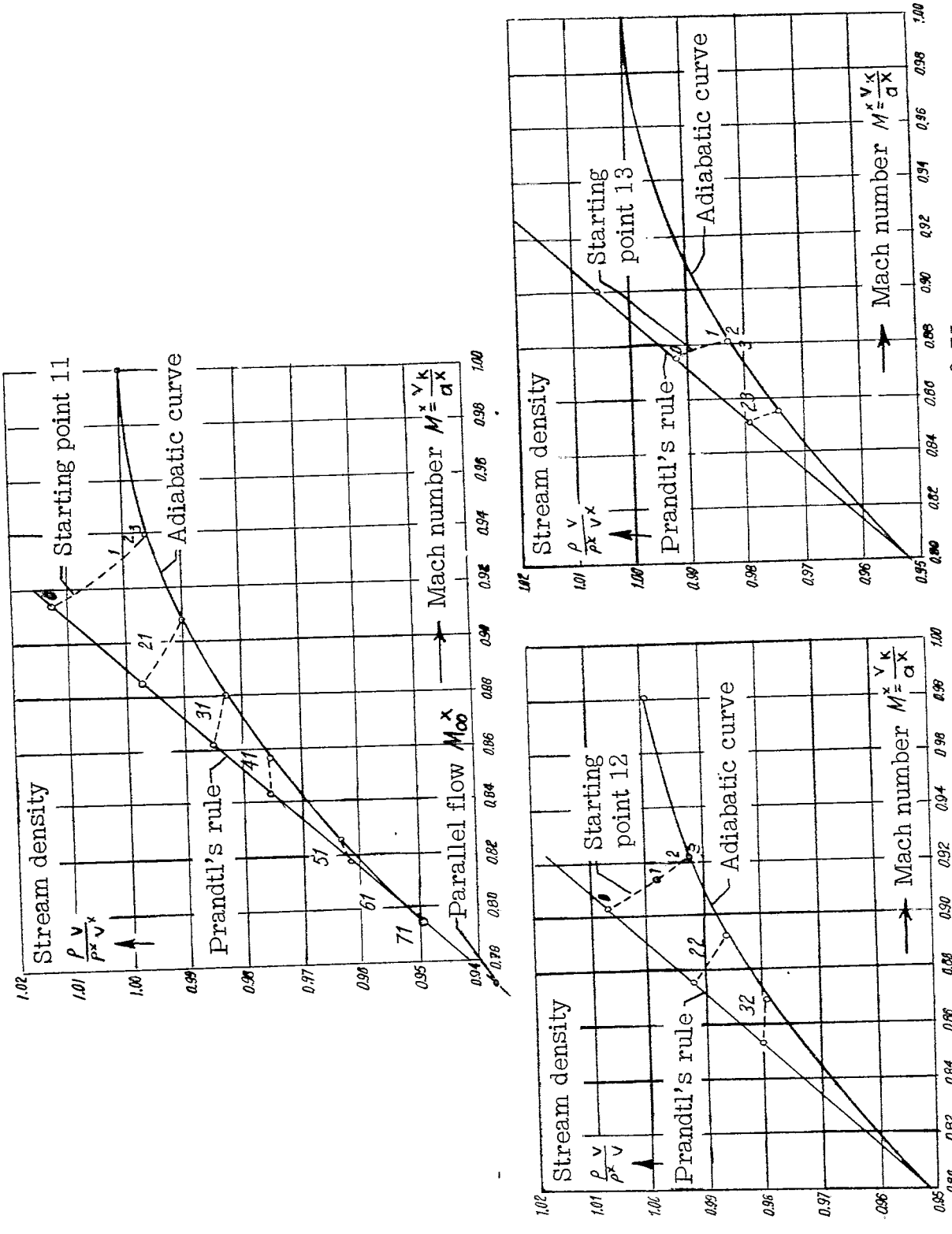

Figure 3.- Line (crescent) (d/l = 0.10), M_∞ = 0.75.
Velocity and stream density for various approximations to the adiabatic curve (source system I).

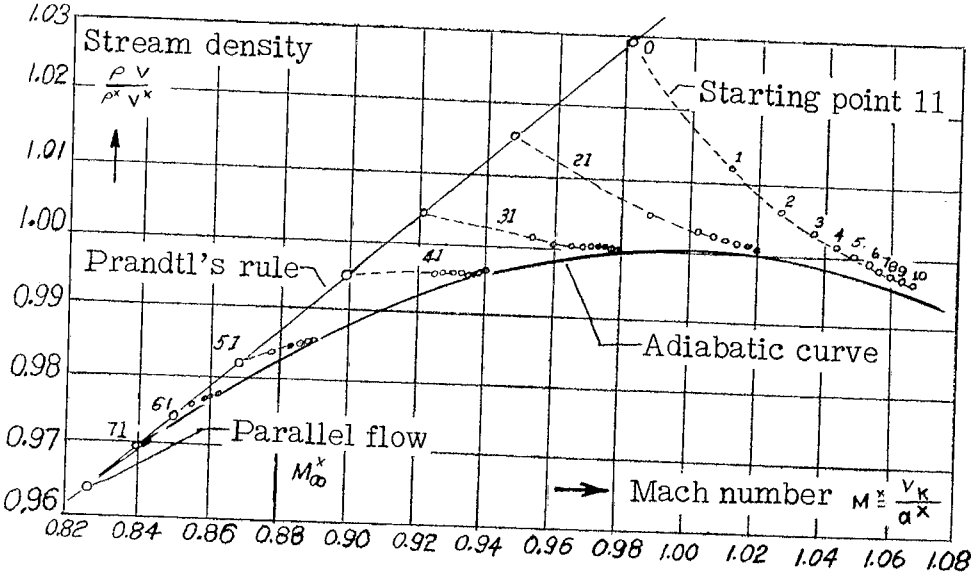

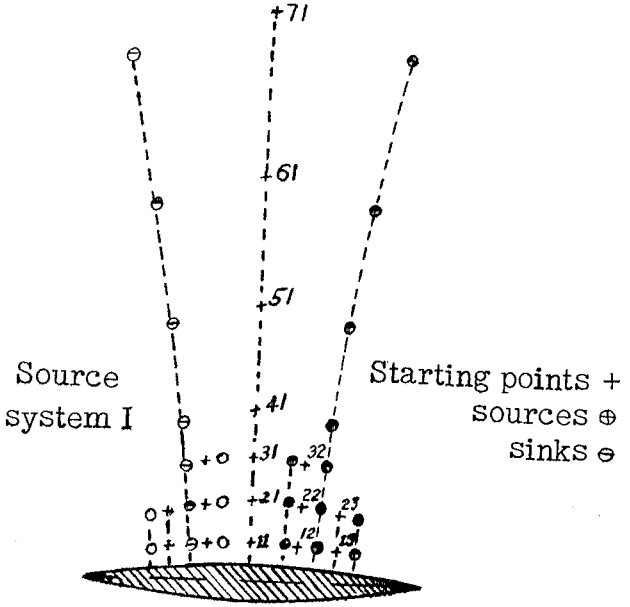

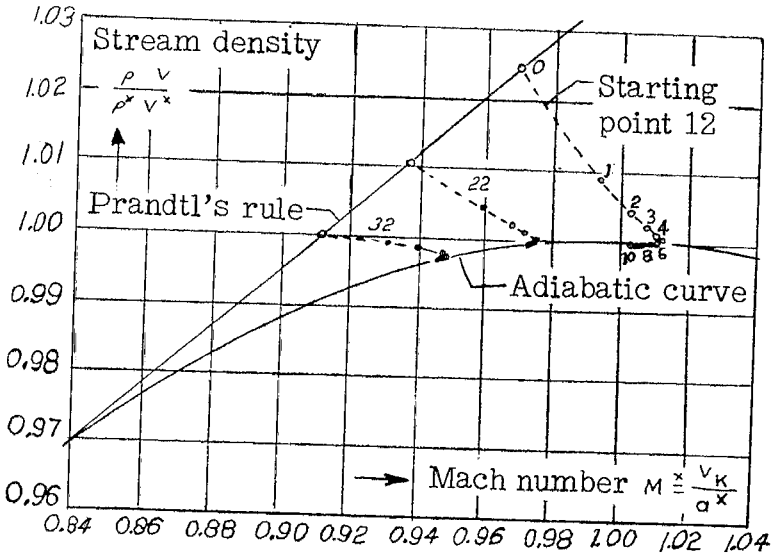

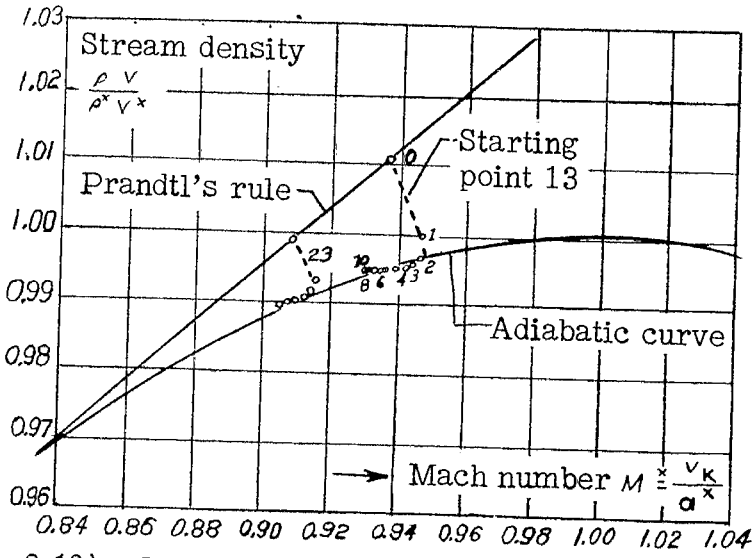

Figure 4.- Line (crescent) ($d/l = 0.10$), $M_\infty = 0.80$.
Velocity and stream density for various approximations to the adiabatic curve (source system I).

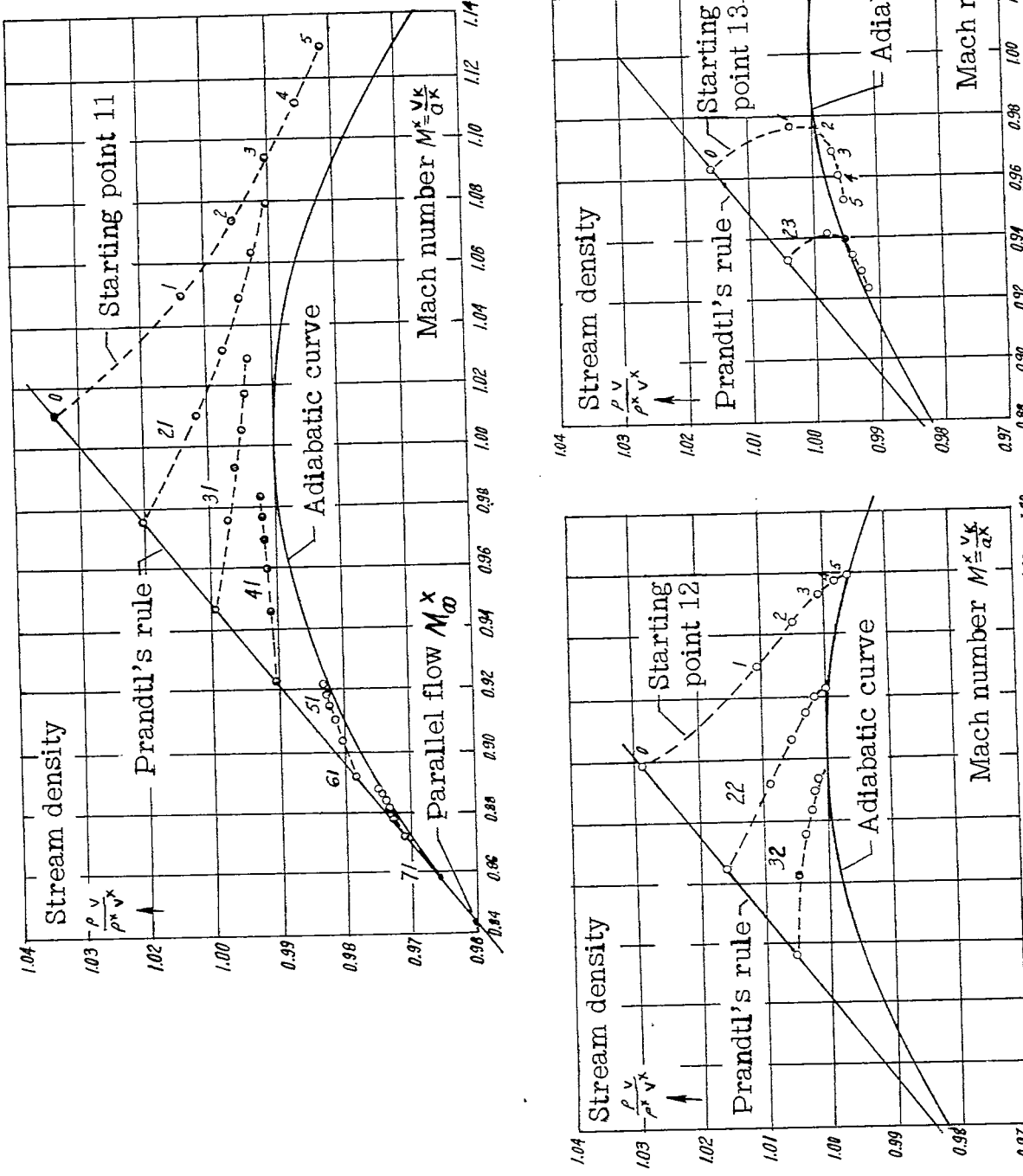

Figure 5.- Line (crescent) (d/l = 0.10), $M_\infty = 0.82$. Velocity and stream density for various approximations to the adiabatic curve (source system I).

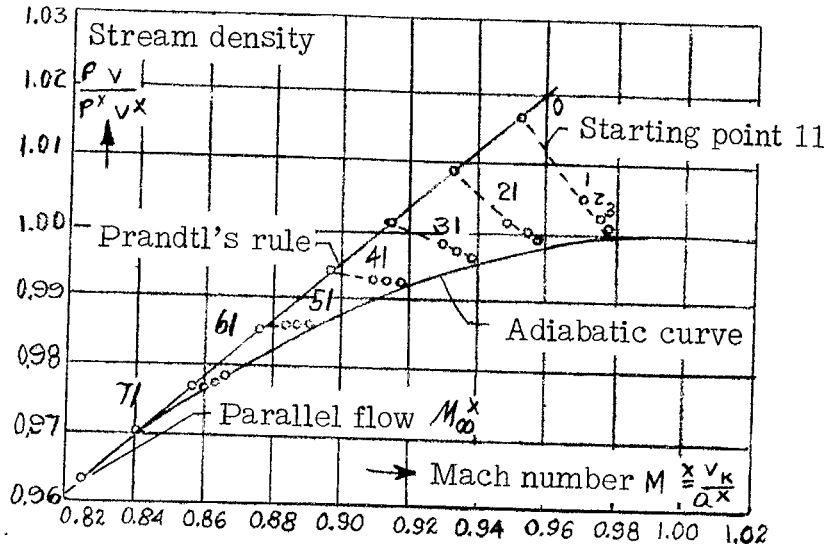

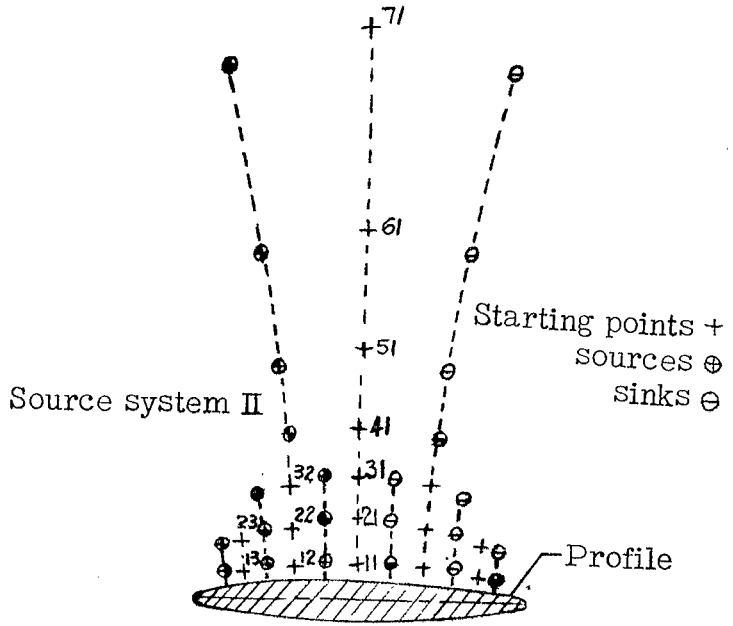

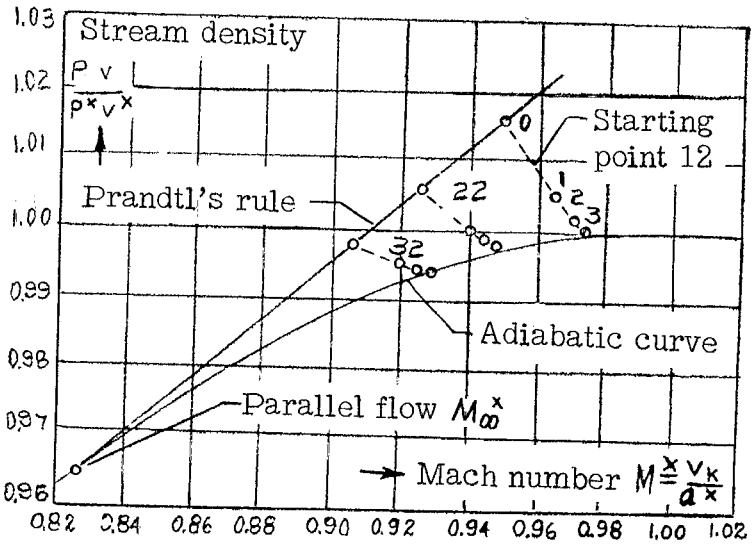

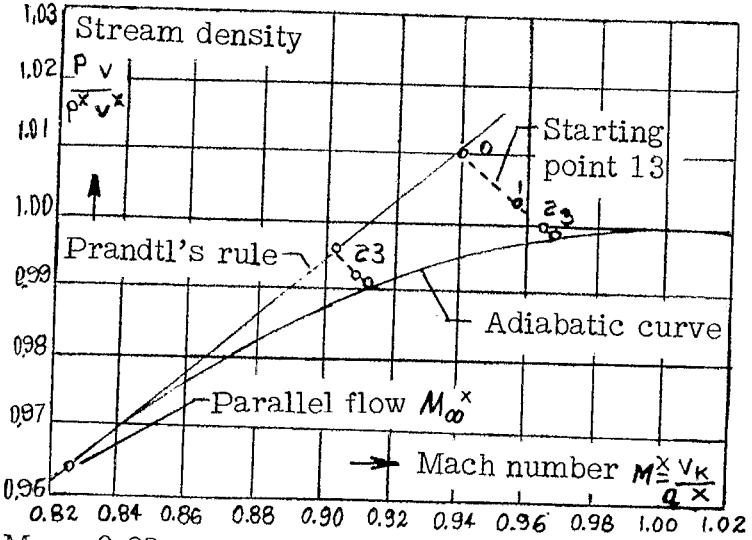

Figure 6.- Ellipse ($d/l = 0.10$), $M_\infty = 0.80$.
Velocity and stream density for various approximations to the adiabatic curve (source system II.)

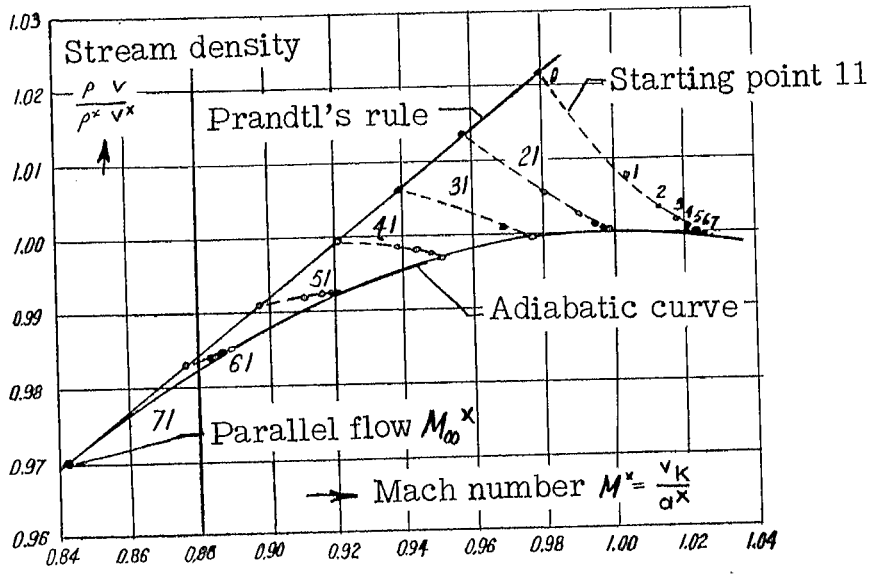

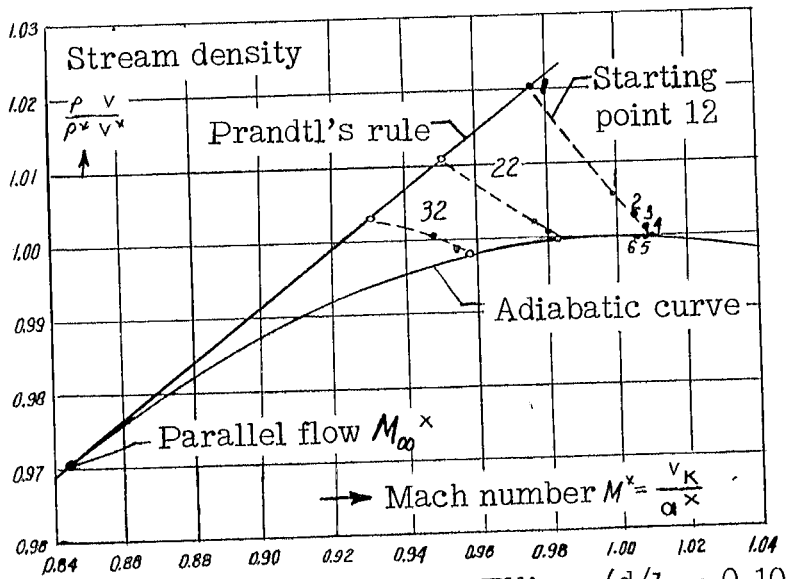

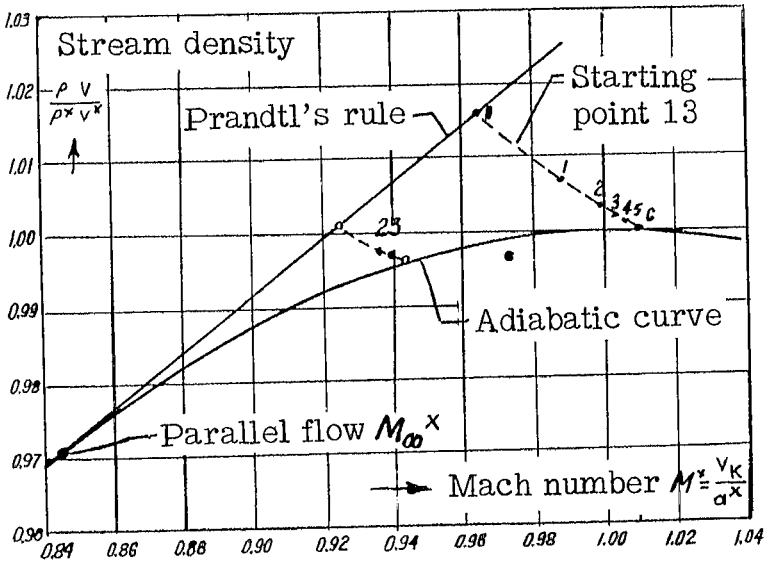

Figure 7.- Ellipse ($d/l = 0.10$), $M_\infty = 0.82$.
Velocity and stream density for various approximations to the adiabatic curve (source system II).

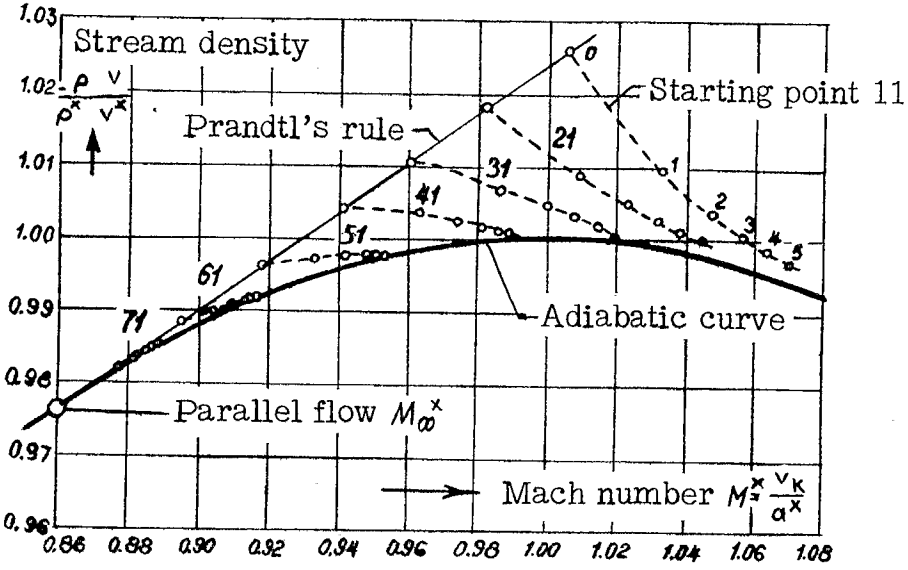

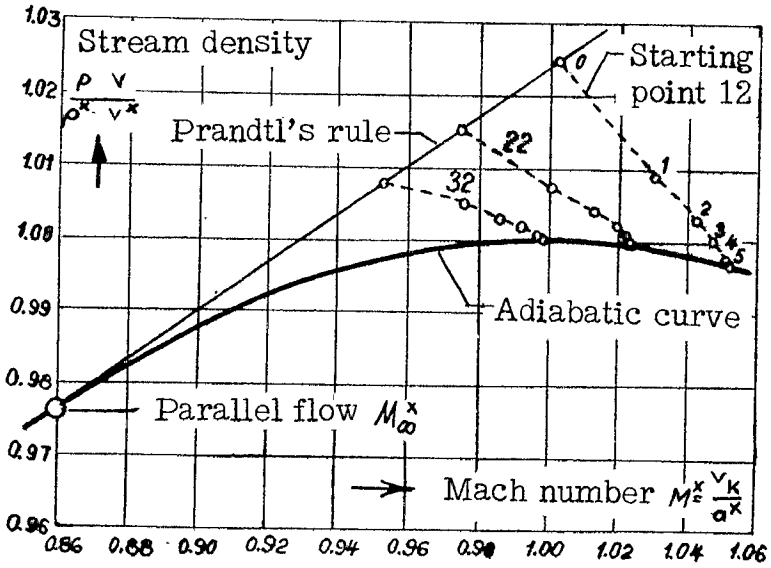

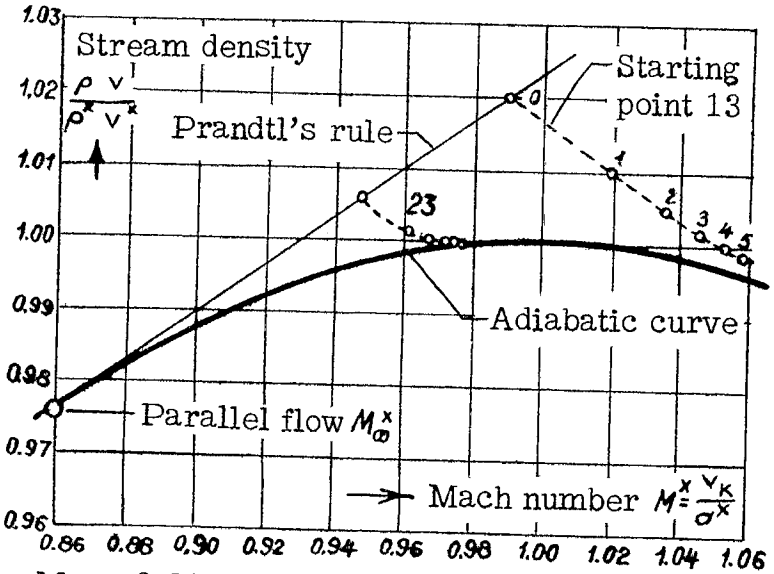

Figure 8.- Ellipse ($d/l = 0.10$), $M_\infty = 0.838$.
Velocity and stream density for various approximations to the adiabatic curve (source system II).

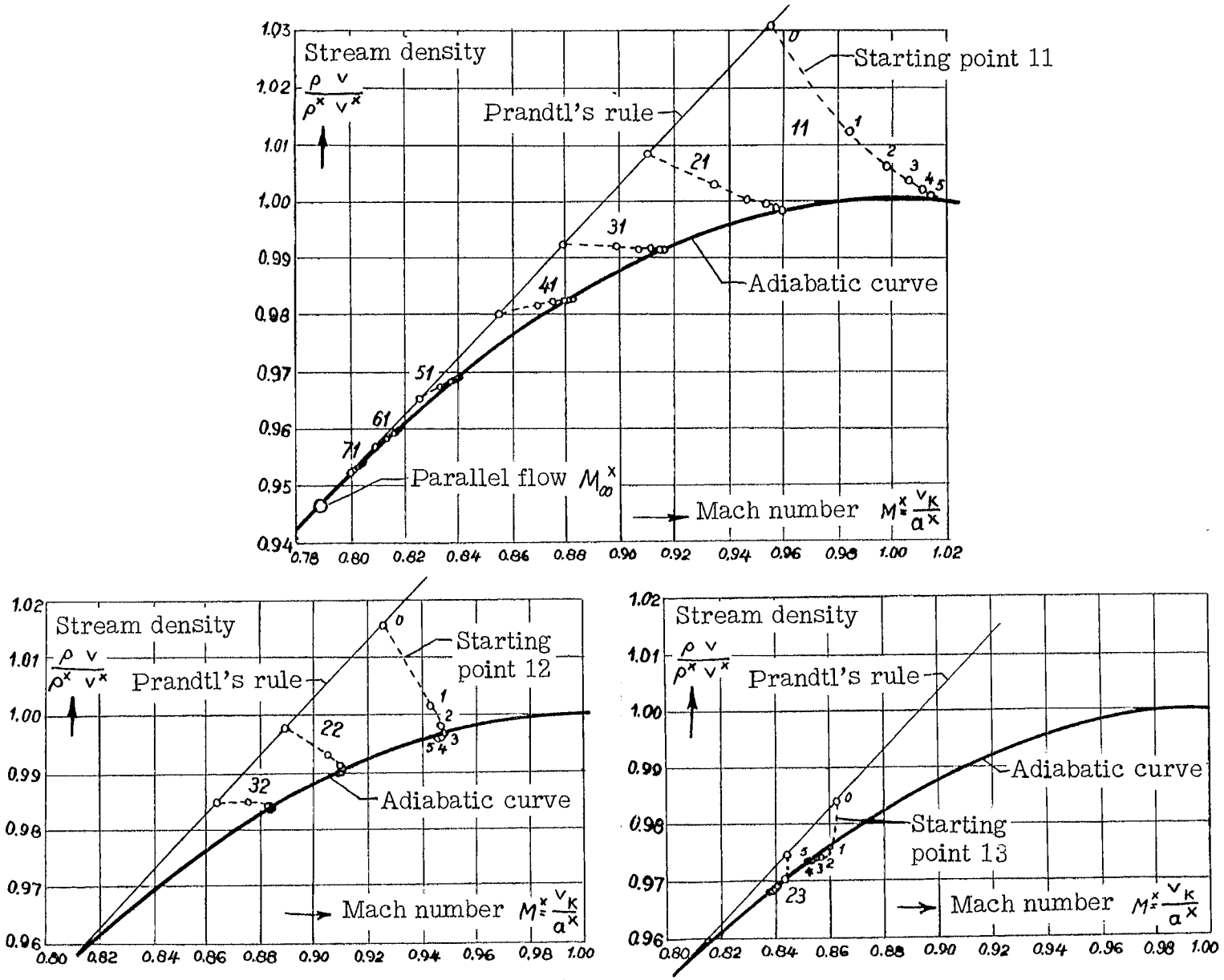

Figure 9.- Spindle-shaped body ($d/l = 0.10$), $M_\infty = 0.76$
Velocity and stream density for various approximations to the adiabatic curve (source system I).

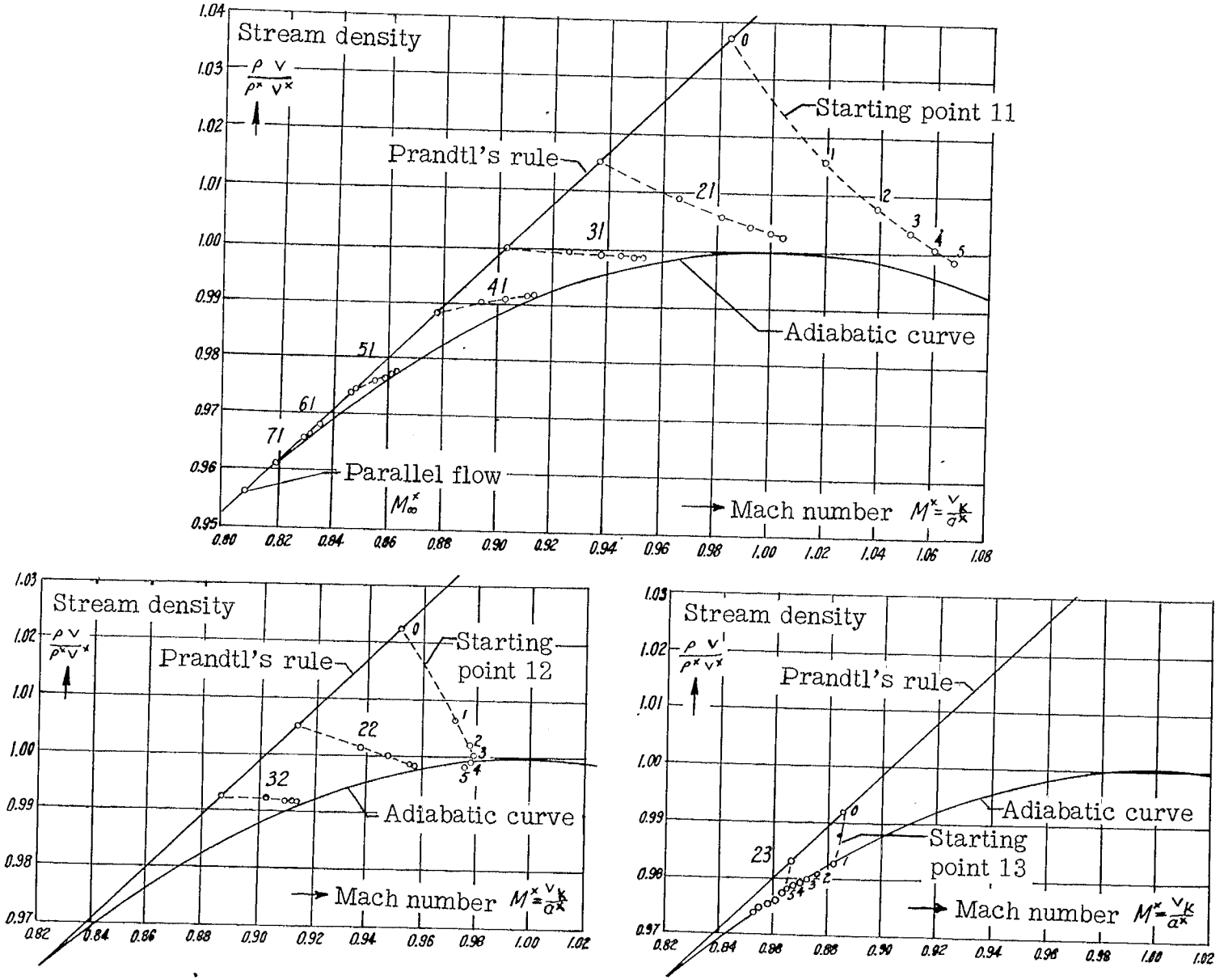

Figure 10.- Spindle-shaped body ($d/l = 0.10$), $M_\infty = 0.78$. Velocity and stream density for various approximations to the adiabatic curve (source system I).

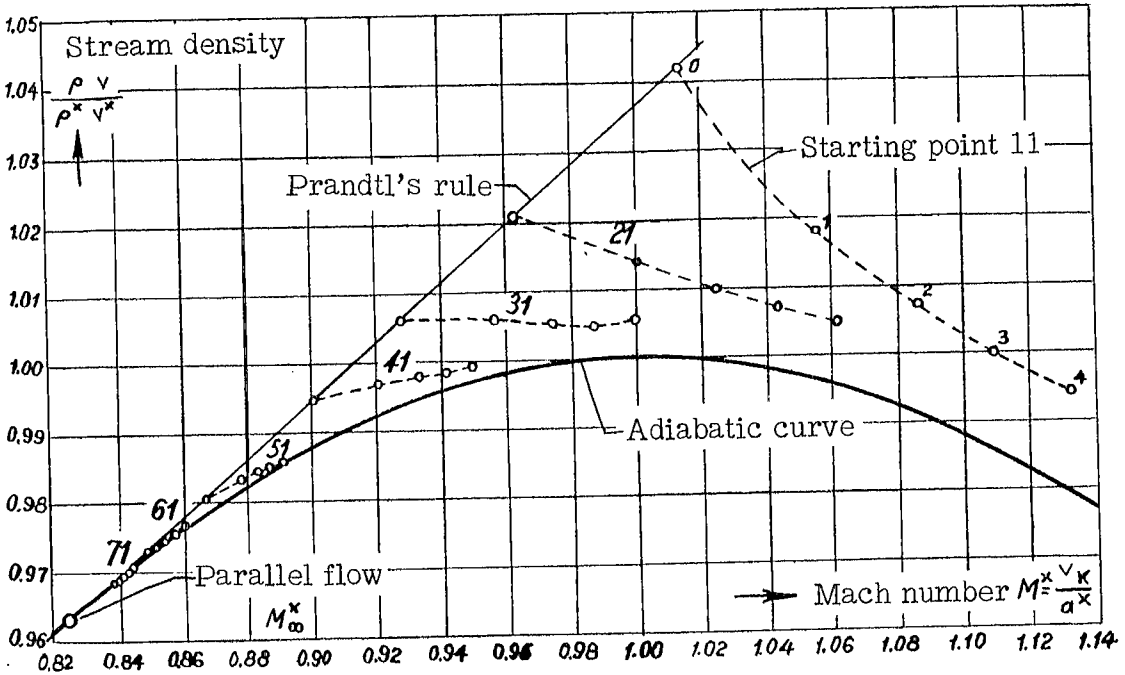

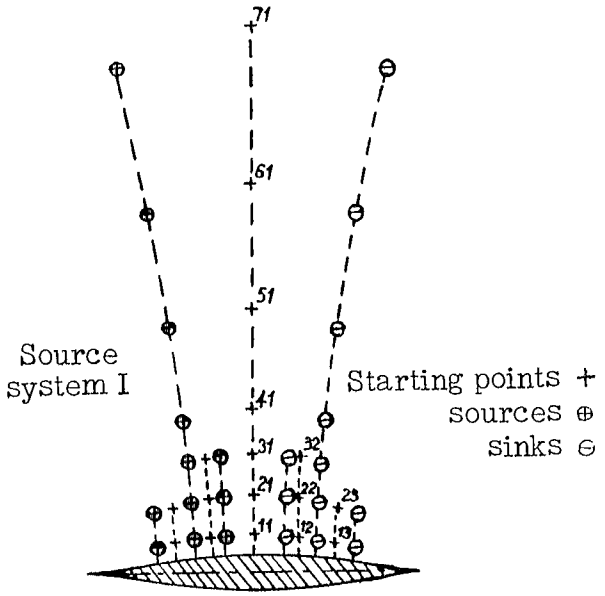

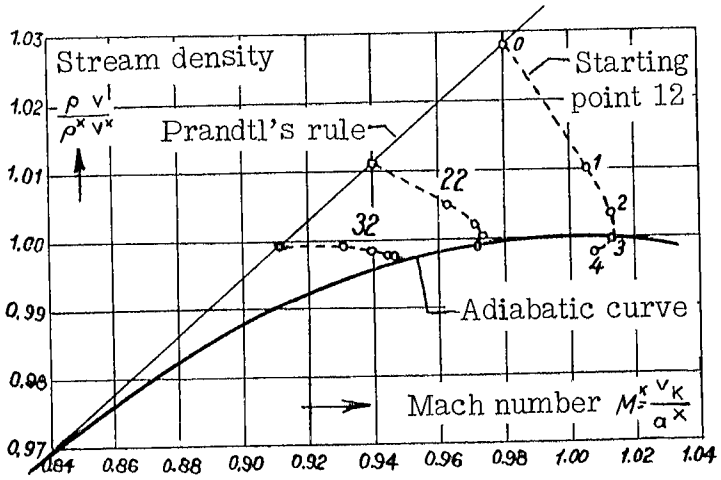

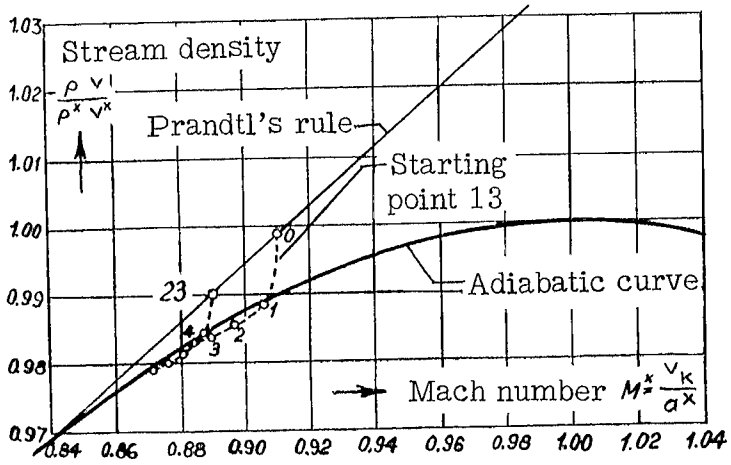

Figure 11.- Spindle-shaped body ($d/l = 0.10$), $M_\infty = 0.80$.
Velocity and stream density for various approximations to the adiabatic curve (source system I).

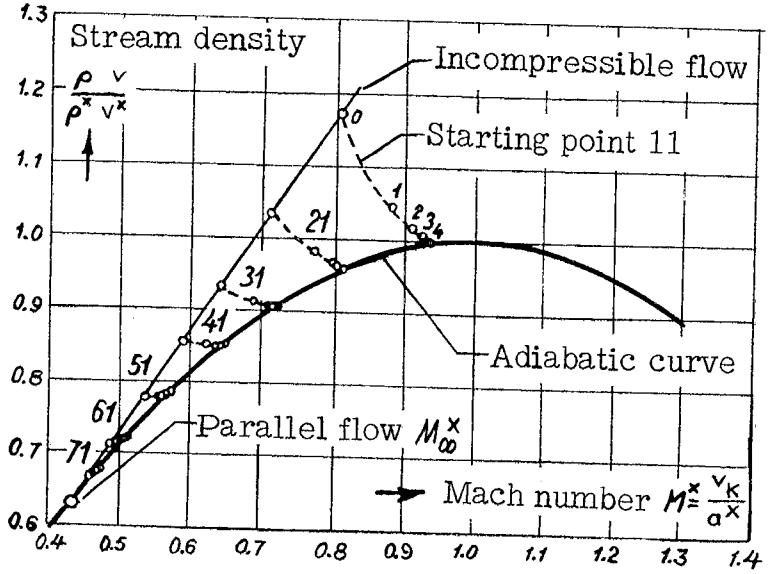

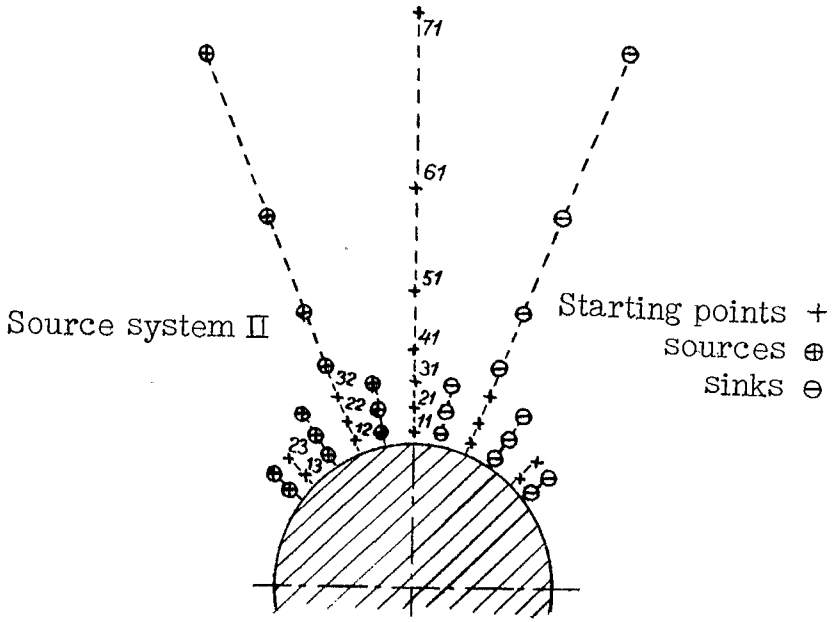

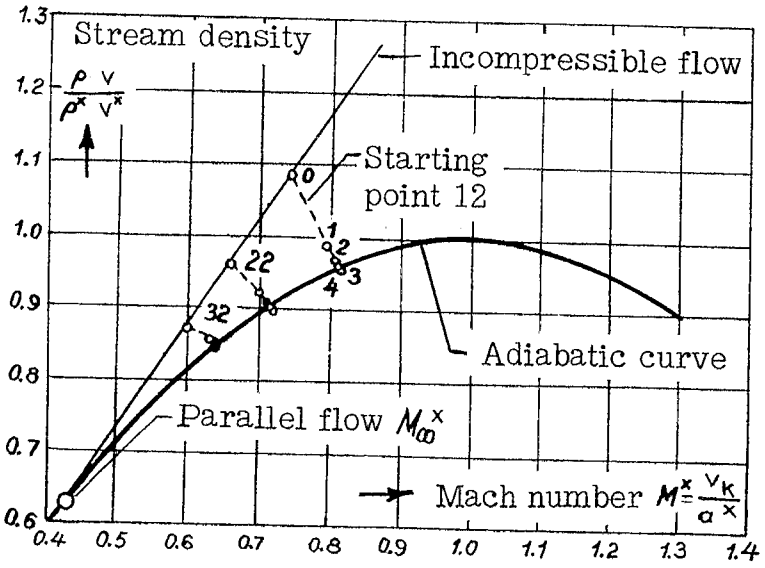

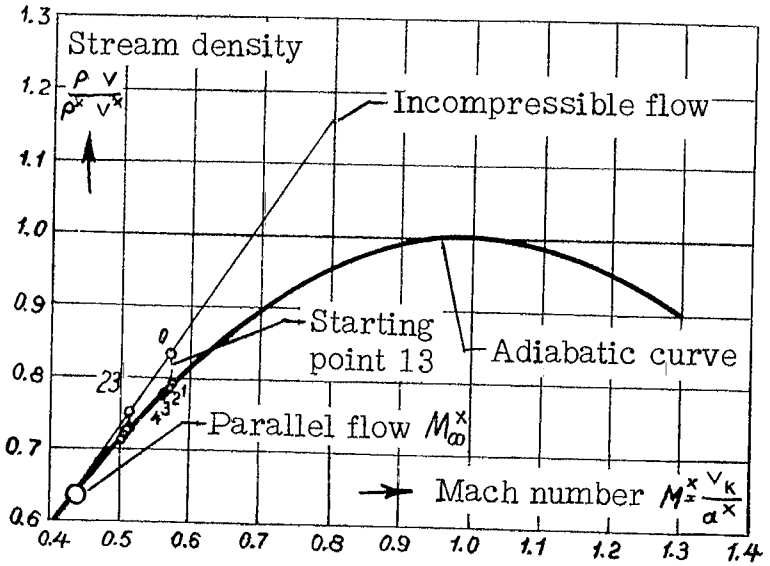

Figure 12.- Circle. $M_\infty = 0.40$.
Velocity and stream density for various approximations to the adiabatic curve (source system II).

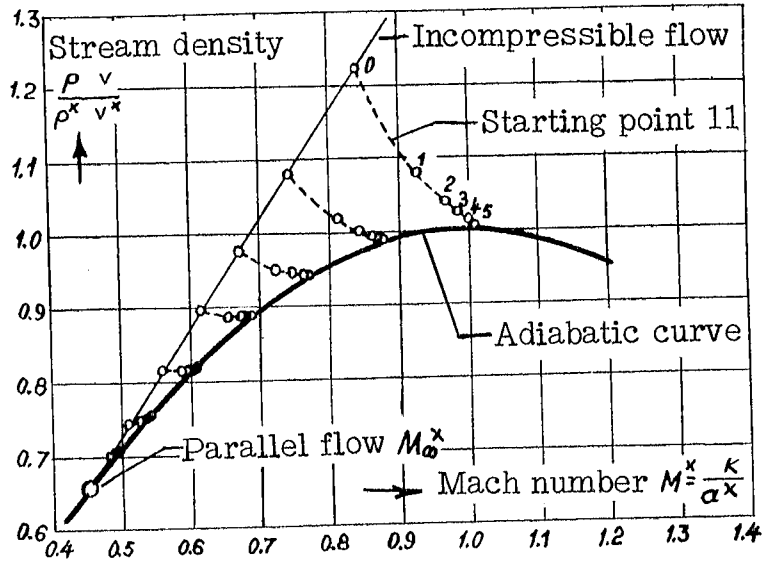

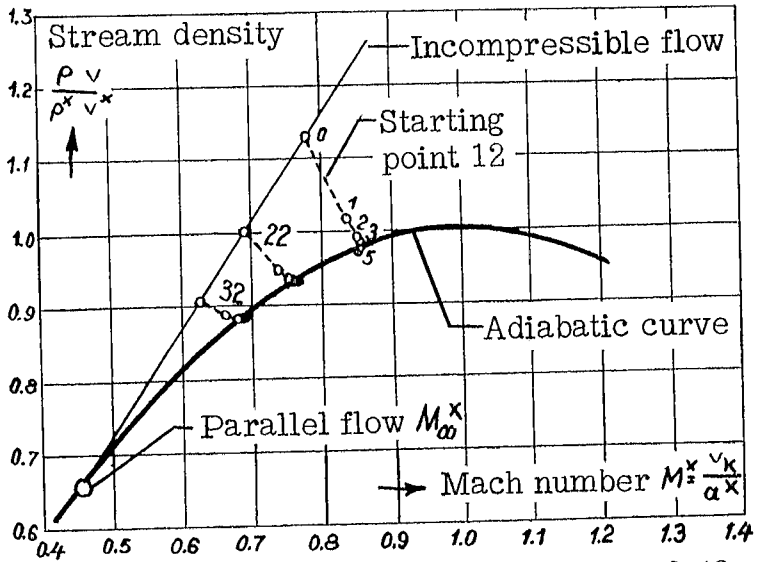

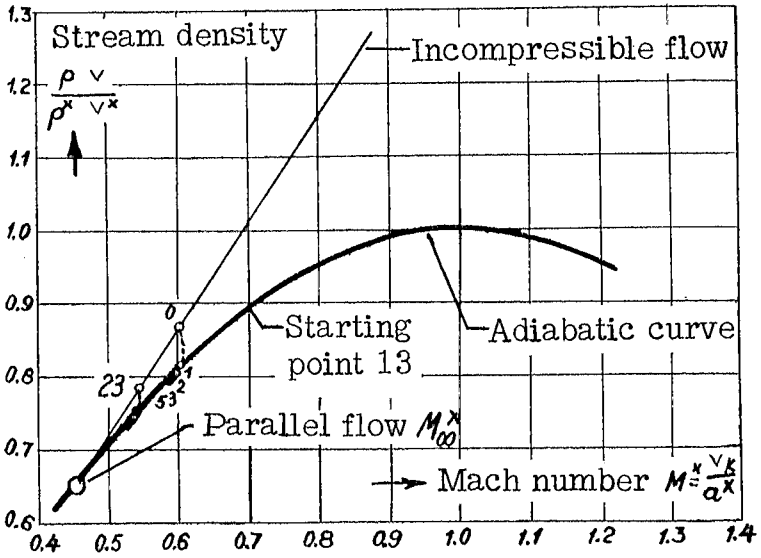

Figure 13.- Circle. $M_\infty = 0.42$.
Velocity and stream density for various approximations to the adiabatic curve (source system II).

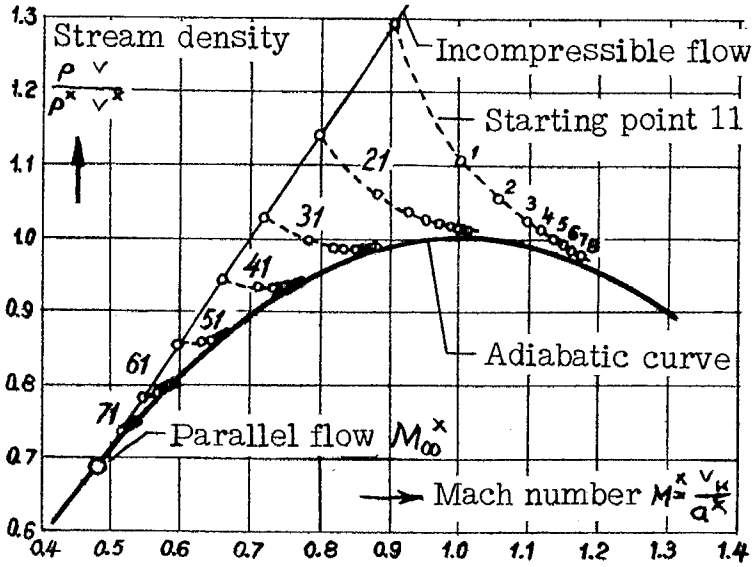

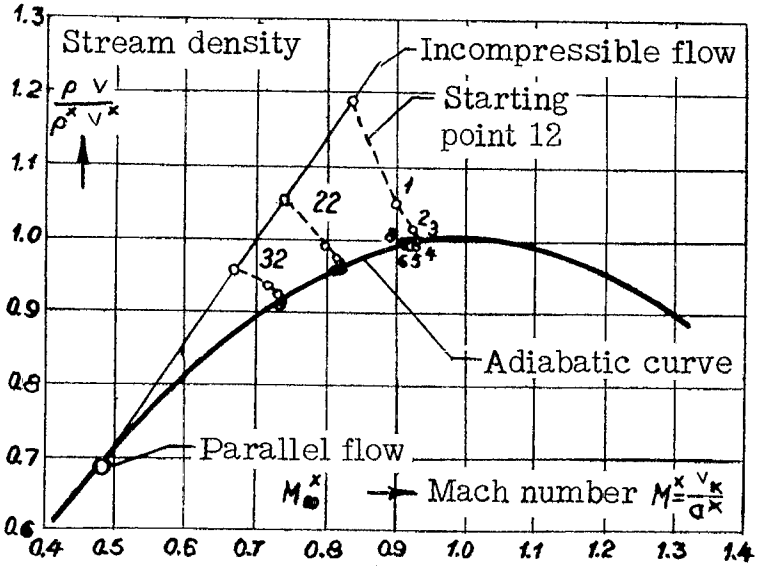

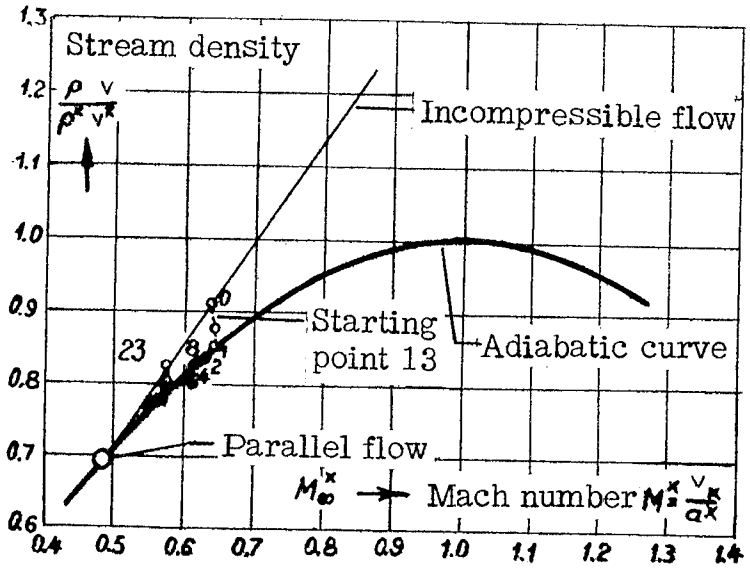

Figure 14.- Circle. $M_\infty = 0.45$.
Velocity and stream density for various approximations to the adiabatic curve (source system II).

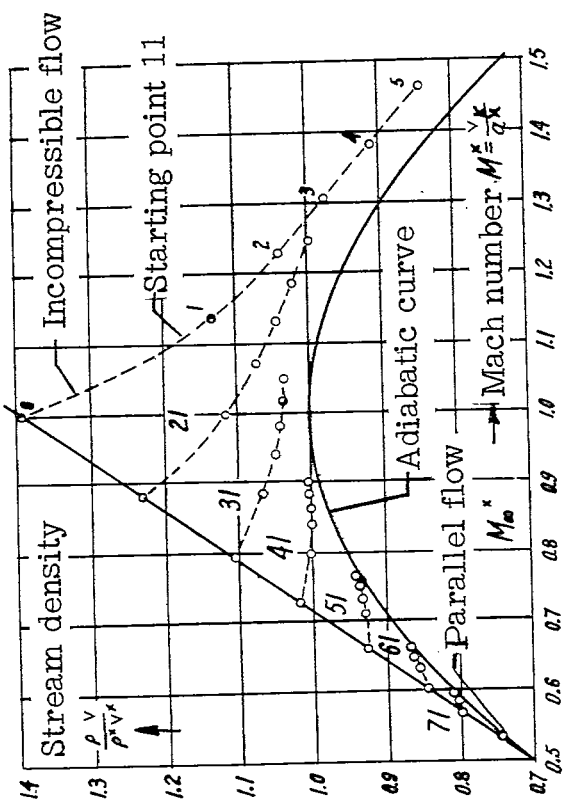

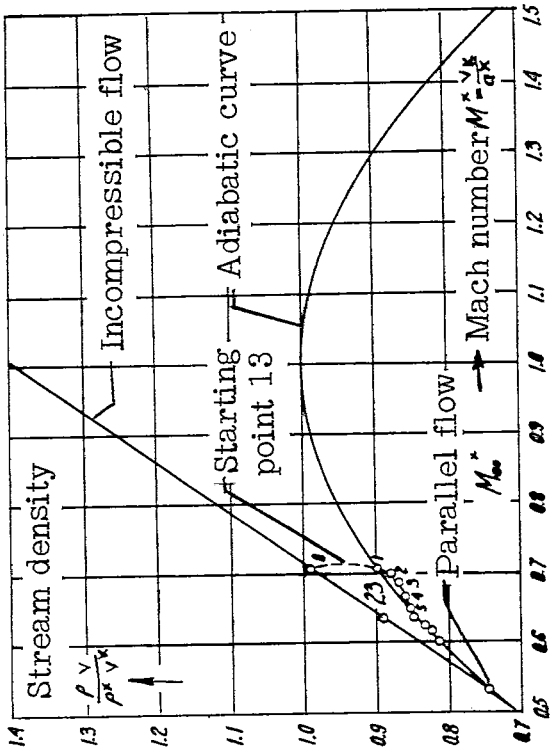

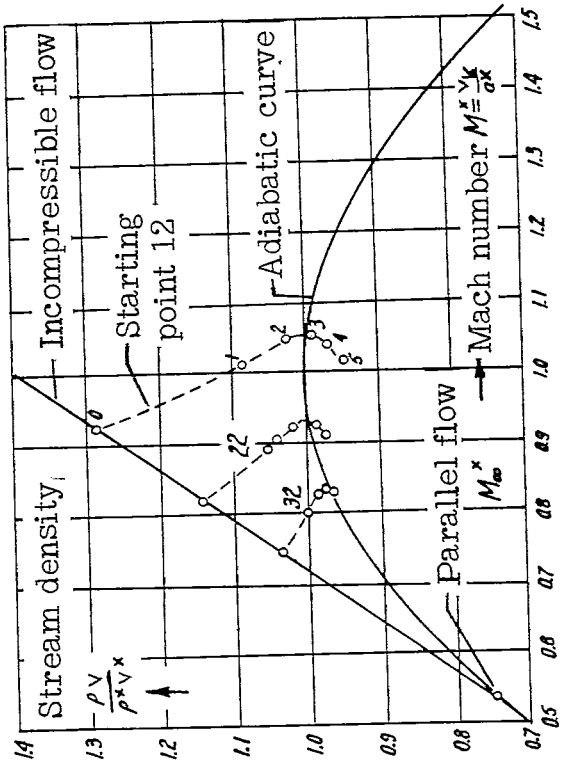

Figure 15.- Circle. $M_\infty = 0.50$.
Velocity and stream density for various approximations to the adiabatic curve (source system II).

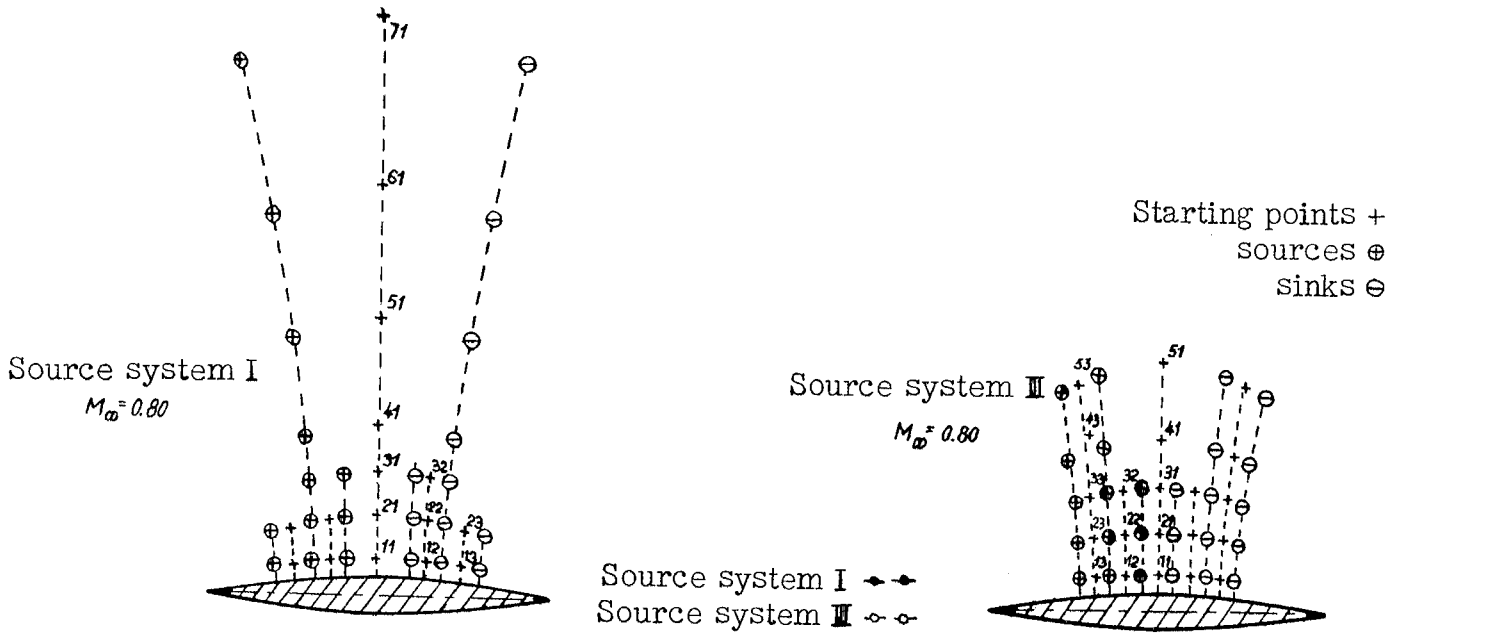

Figure 16.- [Title almost wholly illegible.]
Various . . . . . source systems . . . . . .
. . . . . on the line (crescent) ($d/l = 0.10$).

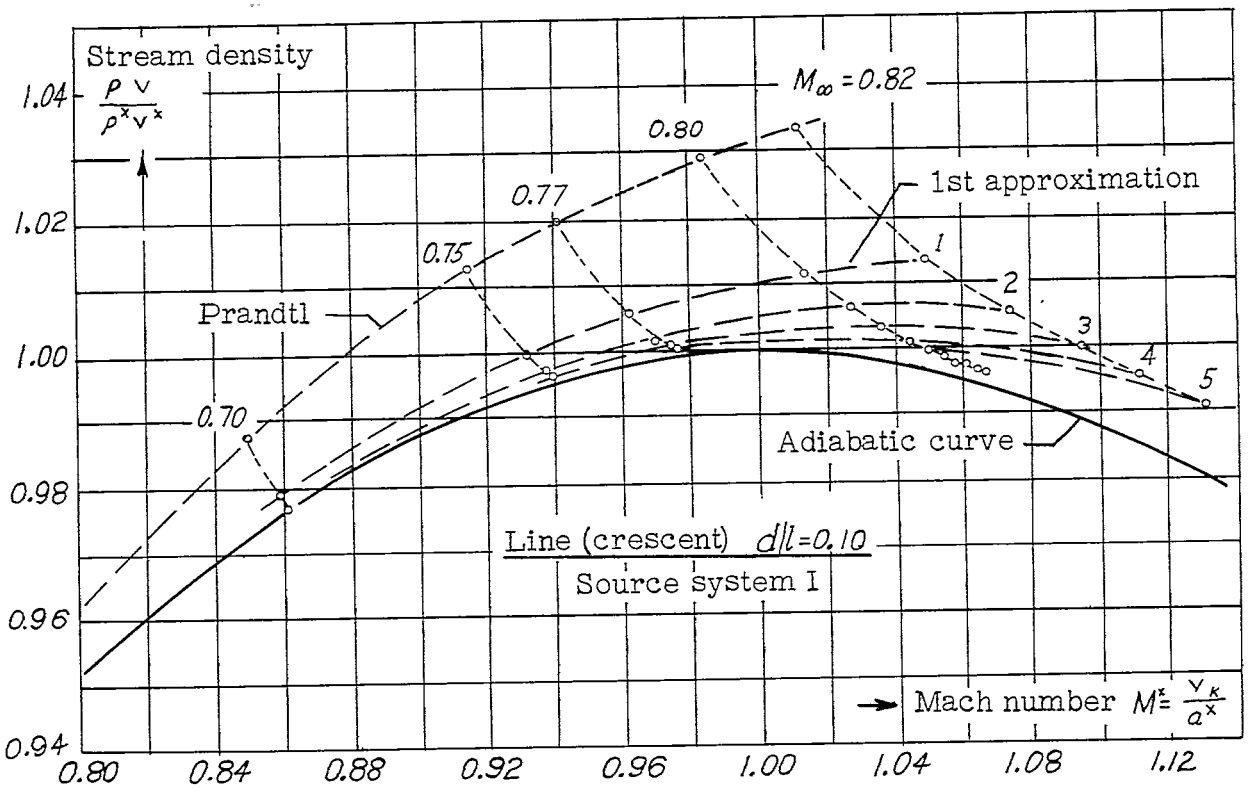

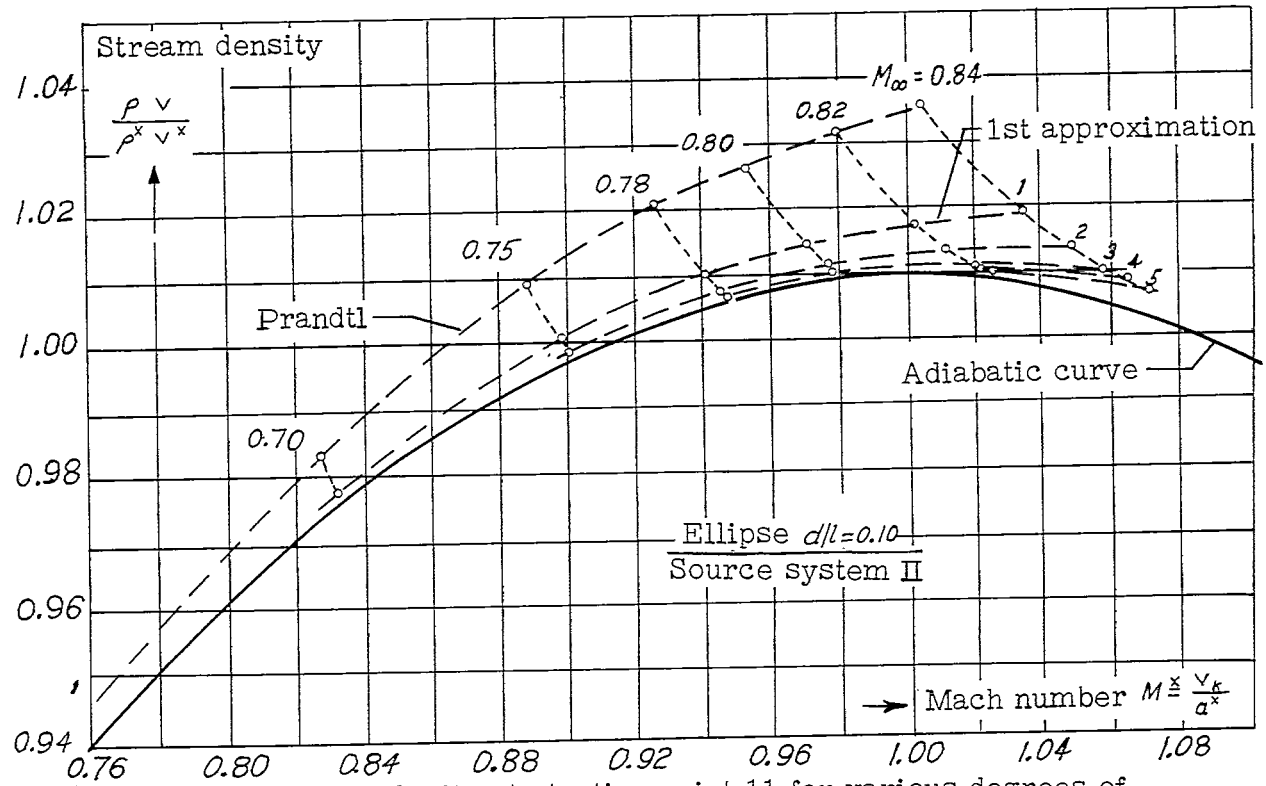

Figure 17.- Velocity at starting point 11 for various degrees of approximation for the line (crescent) ($d/l = 0.10$) and the ellipse ($d/l = 0.10$).

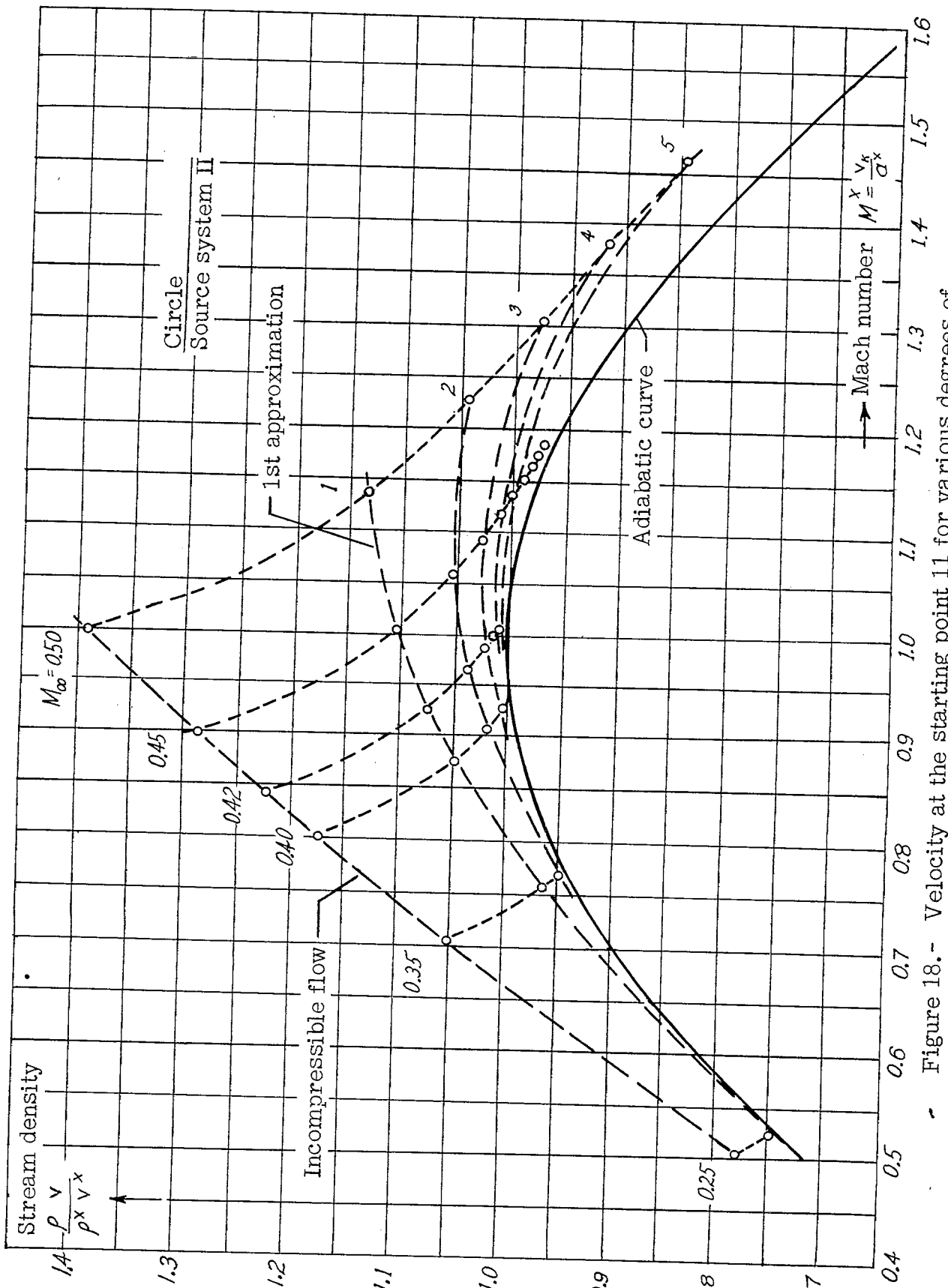

Figure 18.- Velocity at the starting point 11 for various degrees of approximation for the circular cylinder.

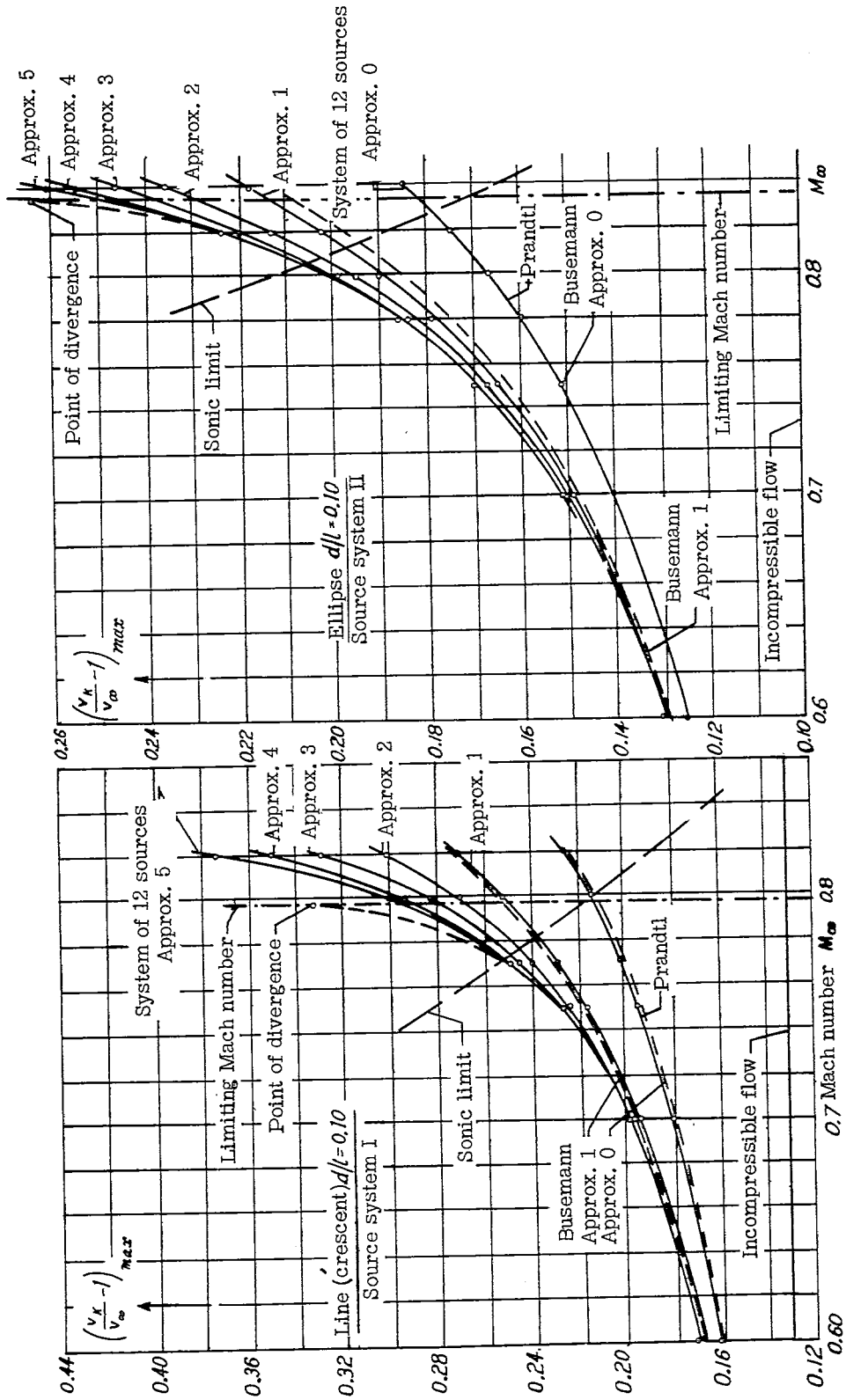

Figure 19.- Maximum excessive velocity $\frac{\Delta v_k}{v_\infty} = \frac{v_k}{v_\infty} - 1$ on the contour according to various approximation calculations for line (crescent) (d/l = 0.10) and ellipse (d/l = 0.10).

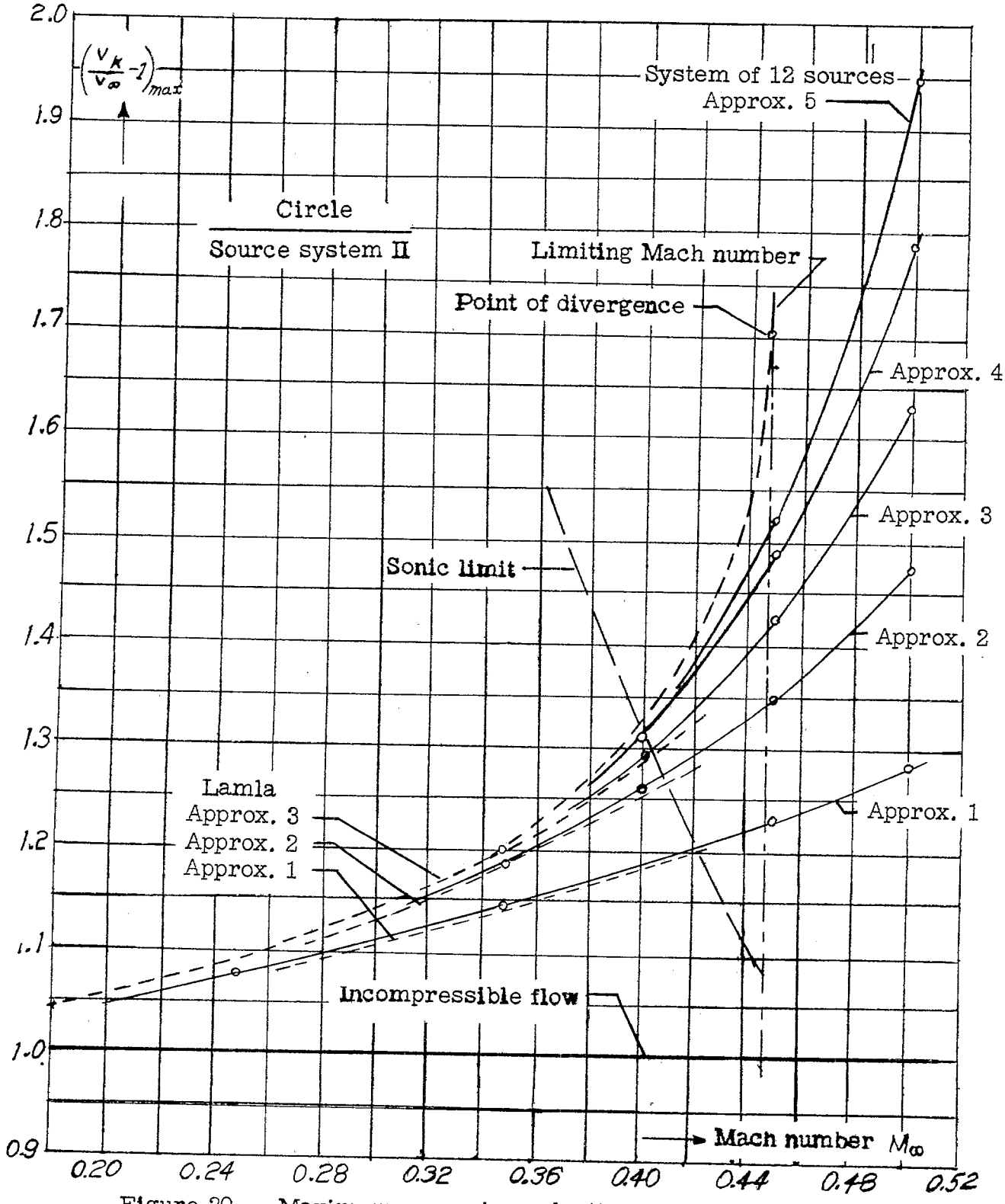

Figure 20.- Maximum excessive velocity on the circle contour according to various approximation calculations.

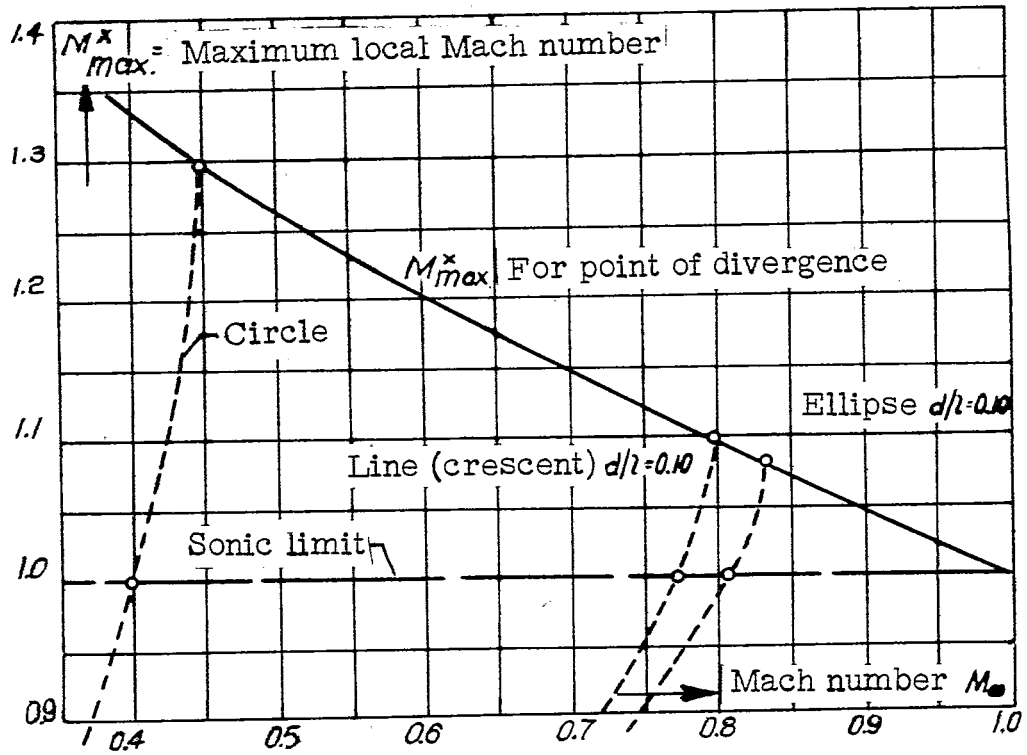

Figure 21.- Maximum local Mach number at the point of divergence as a function of the Mach number of the air velocity.